Nanoscale Horizons

ROYAL SOCIETY OF CHEMISTRY

MINIREVIEW

View Article Online
View Journal | View Issue

Cite this: *Nanoscale Horiz.*, 2021, **6**, 209

Switching to the brighter lane: pathways to boost the absorption of lanthanide-doped nanoparticles

Riccardo Marin,*[a] Daniel Jaque [ab] and Antonio Benayas [ab]*

Received 31st October 2020,
Accepted 15th December 2020

DOI: 10.1039/d0nh00627k

rsc.li/nanoscale-horizons

Lanthanide-doped nanoparticles (LNPs) are speedily colonizing several research fields, such as biological (multimodal) imaging, photodynamic therapy, volumetric encoding displays, and photovoltaics. Yet, the electronic transitions of lanthanide ions obey the Laporte rule, which dramatically hampers their light absorption capabilities. As a result, the brightness of these species is severely restricted. This intrinsic poor absorption capability is the fundamental obstacle for untapping the full potential of LNPs in several of the aforementioned fields. Among others, three of the most promising physicochemical approaches that have arisen during last two decades to face the challenges of increasing LNP absorption are plasmonic enhancement, organic-dye sensitization, and coupling with semiconductors. The fundamental basis, remarkable highlights, and comparative achievements of each of these pathways for absorption enhancement are critically discussed in this minireview, which also includes a detailed discussion of the exciting perspectives ahead.

1. Introduction

Despite suggestions of turning the periodic table upside down,[1] lanthanides (from the Greek word lanthaneien meaning "lying hidden") continue to occupy the bottom part of it together with their bigger brothers, namely actinides. This representation makes lanthanides quite literally "outstanding" elements but not only for their unique properties. Lanthanides, which along with scandium and yttrium form the family of rare earths, are indeed elements of strategic interest for several applications. Anti-counterfeiting tags in banknotes, blue-light conversion layer in LEDs, permanent magnets, and lighter flints are some of the mundane objects containing lanthanides that cross our paths on a daily basis. Other materials are more

[a] *Fluorescence Imaging Group (FIG), Departamento de Física de Materiales, Facultad de Ciencias, Universidad Autónoma de Madrid, C/Francisco Tomás y Valiente 7, Madrid 28049, Spain. E-mail: riccardo.marin@uam.es, antonio.benayas@uam.es*
[b] *Nanobiology Group, Instituto Ramón y Cajal de Investigación, Sanitaria Hospital Ramón y Cajal, Ctra. de Colmenar Viejo, Km. 9100, 28034 Madrid, Spain*

Riccardo Marin

Riccardo Marin obtained his PhD in Chemistry jointly from the University Ca'Foscari (Venice, Italy) and the Institut National de la Recherche Scientifique (INRS-Varénnes, Canada) under the supervision of Prof. P. Canton and Prof. F. Vetrone. He then undertook a postdoctoral fellowship at the University of Ottawa from 2017 to 2019 with Prof. E. Hemmer and Prof. M. Murugesu. He is currently a Marie Skłodowska-Curie fellow at the Universidad Autónoma de Madrid in the group of Prof. D. Jaque. His research interests encompass the development and study of optically active (nano)materials based on lanthanide ions and semiconductors.

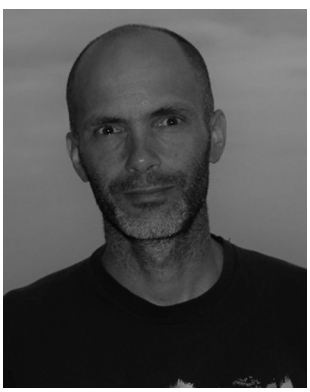

Daniel Jaque

Daniel Jaque got his PhD in Physics from Universidad Autónoma de Madrid (UAM, Spain) in 1999. After a decade of outstanding research on laser materials and photonics, he founded the Fluorescence Imaging Group together with Prof. J. García Solé in 2010, which has been working to develop luminescent materials nanomaterials of different kinds (quantum dots, lanthanide doped nanoparticles, etc.) towards applications ranging from optical trapping to biomedical imaging. Prof. Jaque was a pioneer from the dawn of luminescence thermometry; today, he is a world-renowned leader in the in vivo application of this technique.

exotic, such as lanthanide complexes behaving as magnets at the single-molecule level (single-molecule magnets-SMMs).[2,3] However, herein, we are interested in a particular family of materials that capitalize on the light emitted by trivalent lanthanide ions (Ln^{3+}); colloidal nanoparticles doped with Ln^{3+} (LNPs). LNPs are the workhorses in several fields of nanotechnology owing to their capability, for example, to act as optical probes[4–6] and photo-initiate chemical reactions under excitation with low-energy photons.[7,8] The small size of LNPs makes them usable in microenvironments (*e.g.*, cells)[9] and more generally for the investigation of phenomena with sub-micrometric accuracy while minimally perturbing the observed system.[10,11] They have also been proposed for the preparation of light harvesting layers for low-energy photons, which would otherwise go unexploited in photovoltaic devices.[12,13] All in all, LNPs have deservedly gained a place of respect in the field of nanotechnology alongside their older kin featuring photoluminescence properties—the family of semiconductor nanocrystals. LNPs and semiconductor nanocrystals are both inorganic luminescent nanoparticles. However, the similarities between them end there. Numerous discrepancies exist in terms of chemistry and physics, making each of these nanomaterials suited for specific applications where the other might need to stretch. Hence, LNPs and semiconductor nanocrystals are complementary rather than competing both with their advantages and shortcomings. Speaking of the latter, the most notable limitation of LNPs resides in their low overall emission intensity, which is the result of the electronic configuration of Ln^{3+} ions (*vide infra*). This poor brightness represents a major bottleneck in the widespread employment of LNPs in fields such as lighting and optical imaging. However, brighter LNPs would also translate to better performance in applications where these species are already routinely employed, such as in the field of sensing. Given the central role played by brightness in the context of this minireview, it is convenient to provide its rigorous definition from the very beginning, *i.e.*, the product of molar absorption coefficient and photoluminescence quantum yield (PLQY). In layman terms, these two quantities define the efficiency of a species in absorbing and emitting photons.

In this review, we discuss the recent advances in the development of brightly-emitting LNPs through the improvement of their absorption. In Section 2, we present in simple and comprehensive terms the "brightness issue" that affects Ln^{3+} luminescence. We then proceed to Section 3 to critically review the methods developed so far for tackling this issue. Although several approaches have been proposed, we herein focus on three specifically: the use of plasmonic moieties to increase the absorption (and emission) prowess of Ln^{3+}, and the sensitization of Ln^{3+} emission through the use of organic dyes and semiconductors. Lastly, in Section 4, we provide an overview of the field, pinpointing the questions still unresolved, also identifying the most promising and probable future research directions.

2. Lanthanide ions and their forbidden transitions

Trivalent lanthanides (Ln^{3+}) owe most of their properties to non-bonding electrons occupying the 4f orbitals.[14,15] Precisely because of this lack of involvement of 4f electrons in the formation of bonds, at the single-ion level, Ln^{3+} feature remarkably similar physical properties *in vacuo* and when bound to other elements to form compounds. The "ladder" of the 4f electronic states of each Ln^{3+} (Fig. 1) is in fact screened by external charge densities from the 5s and 5p orbitals. Thus, the electrons can jump undisturbed between the steps of the 4f ladder; however, they should obey an important quantum mechanics constraint, namely, the parity (Laporte) rule.[16] This rule states the impossibility of electronic transitions between states with the same parity (such as 4f–4f intraconfigurational transitions) to occur in centrosymmetric environments. Fortunately, even when a Ln^{3+} is placed at the centre of a perfectly centrosymmetric coordination polyhedron, f–f electronic transitions can still occur thanks to vibrations that induce a temporary reduction of the symmetry. Moreover,

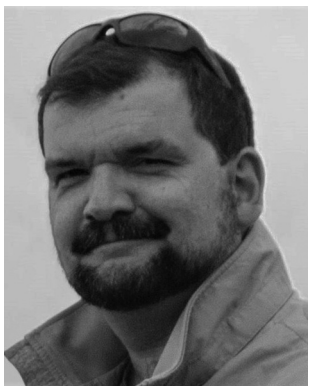

Antonio Benayas

Antonio Benayas was awarded his PhD "cum laude"—Physics of Light and Matter—at Universidad Autónoma de Madrid (UAM, Spain) in 2012. His research then shifted to near-infrared emitting luminescent nanoparticles, supported by health-related funding agencies to join the group led by Prof. Vetrone (INRS, Canada). Later on, he worked at Stanford School of Medicine (USA) with Prof. J. Rao, and at Aveiro Materials Institute (CICECO, Portugal) joining forces with Prof. L. Carlos; both of those terms were supported by a Marie Skłodowska-Curie Action (European Commission). By mid-2020 Dr Benayas joined his alma mater (UAM), thus starting a tenure-track contract.

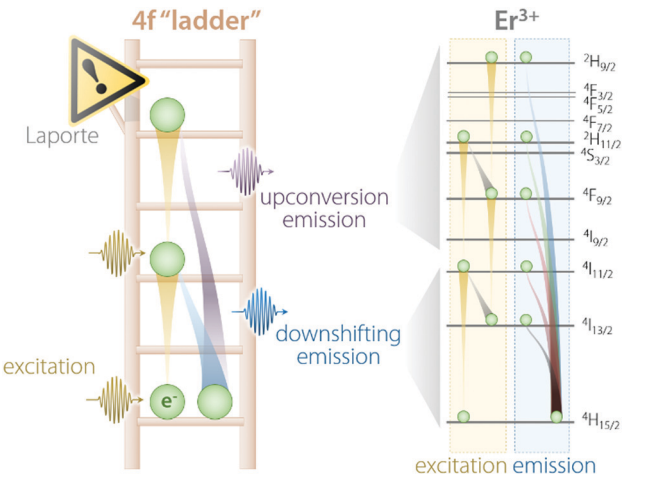

Fig. 1 Schematic representation of the "4f ladder" featured by Ln^{3+} ions, along with the real example of Er^{3+} excitation and emission processes under 980 nm excitation.

admixing with opposite-parity wavefunctions (*e.g.*, 5d orbitals and/or coordinating ligands) can also cause the breakdown of this selection rule. Of course, the forbidden nature of these transitions decreases the probability of an electron to be excited to a higher-energy state as well as relax to a less energetic one. Therefore, when (and if) an electron is promoted by the absorption of a photon to a higher step of the ladder, it will sit there for a relatively long time (micro- to milliseconds) before being kicked up to an even more energetic state or relaxing to a lower lying one. Under the right conditions, such relaxation is accompanied by the release of energy in the form of a photon whose energy matches the energy difference between the initial and final states, rather than as heat generated by vibrations. Overall, the unique electronic configuration of Ln^{3+} results in emissions that are narrow (atom-like), fall at relatively constant energies (changing by few hundred wavenumbers at most), and have extended lifetimes. The long-lived nature of the 4f electronic states is desirable since it can be harnessed to generate the optical phenomenon of upconversion (UC). This process entails the sequential absorption of multiple low-energy photons, followed by radiative relaxation of the excited electron with the emission of a single higher-energy photon.[17]

However, the reduced probability of these transitions also translates to poor light absorption and thus to low brightness. From an optical standpoint, this is the more relevant shortcoming of Ln^{3+} ions since it limits the effectiveness of the direct excitation of 4f electrons responsible for emission. Quantitatively, the capability to absorb a photon of specific energy (*i.e.*, wavelength) is defined by the molar extinction coefficient, which is expressed in units of length per mole. This parameter is of the order of 0.1–10 M^{-1} cm^{-1} for Ln^{3+}, while semiconductor nanocrystals and organic dyes feature much larger values in the 10^4–10^6 M^{-1} cm^{-1} range. The product of this parameter and the PLQY (# of emitted photons per # of absorbed photons) gives the brightness of a species, as previously defined. This is arguably the most important parameter to consider for practical uses as it provides an estimate of how much of the excitation light shined on the luminescent species will eventually be converted to emitted light. However, not all Ln^{3+} are the same. Some, such as Nd^{3+} and Yb^{3+}, can absorb light more effectively than others and are thus used as sensitizers, *i.e.*, ions that absorb the excitation light and transfer this energy to the emitting ion (activator). The use of sensitizer–activator pairs is at the basis of the preparation of LNP with good emission brightness. However, more sophisticated strategies have been developed to improve on this concept. In the next section, we discuss selected approaches for the enhancement of this parameter in nanoparticles doped with Ln^{3+} ions, which aim at increasing the excitation light absorption capability of the nanostructure.

To complete this brief overview of the absorption capabilities of Ln^{3+}, it should be noted that there are exceptions to the cases discussed thus far. Among others, Ce^{3+} and Eu^{2+} (divalent europium) are the most relevant lanthanide ions that feature 4f–5d electronic transitions. These transitions are allowed and, as such, yield relatively good light absorption.[18,19] Therefore, in such instances, the ''brightness issue'' is a less urging concern.

3. Strategies to enhance the brightness of Ln^{3+} nanophosphors

Several researchers have been working on the optimization of LNP-based nanosystems with the goal of maximizing the amount of light absorbed and the fraction of energy funnelled to the activator ion (Fig. 2). This effort resulted in the development of several approaches. Some of them entail the introduction of lattice distortion-inducing ions (Fig. 2A)[20–22] and preparation of multi-shell structures (Fig. 2B).[23–28] The former approach aims to manipulate the crystal field experienced by the Ln^{3+} ion, increasing the f–f electronic transition probabilities by the partial admixing of 4f wavefunctions with opposite-parity ones (*i.e.*, 5d orbitals). The latter approach is instead underpinned by concepts such as the maximization of sensitizer concentration, spatial segregation of ions, and surface passivation of the LNP. These approaches push the limit of intrinsic Ln^{3+} optical properties and are not discussed in the present review; the interested reader is encouraged to read the above cited works. Another strategy entails the co-doping of Ln^{3+} with ions featuring allowed electronic transitions, such as Ce^{3+},[29,30] Bi^{3+},[31] and $Mn^{3+/4+}$,[32] which can more effectively absorb light and transfer it to nearby activators (Fig. 2C). These allowed electronic transitions occur with the involvement of orbitals that participate in the formation of chemical bonds, unlike the previously mentioned 4f orbitals. For this reason, the energy of the associated electronic levels (and thus the absorption range) can be tailored *via* the selection of the host material and/or tuning of its composition.[18] These ions can also introduce additional energy levels that act as intermediate states for the population of Ln^{3+}, thus increasing the energy transfer efficiency and enabling the fine tuning of the emission colour. In this review, we do not examine these approaches.

In the following sections, we focus our attention on three strategies. One of them acts *via* the enhancement of the intrinsic absorption (and emission) probability of the Ln^{3+} ions doped into a material, *i.e.*, the use of plasmonic nanostructures (Fig. 2D). The other two rely on light harvesting moieties of different nature—organic dyes (Fig. 2E) and semiconductor nanocrystals (SNCs – Fig. 2F). For each strategy, we outline the general principle at its basis, passing then to the description of the involved physical processes and the listing of the requirements to be met to successfully prepare a brightly emitting colloidal LNP following the selected strategy.

3.1. Plasmonic enhancement

Among the alternatives discussed in this review, the use of plasmonic materials is by far the most explored pathway for the enhancement of LNPs' emission. A plasmon is a quasiparticle that defines the collective motion of free charge carriers within a conductor material (*e.g.*, metals), which occurs at a frequency characteristic of the material itself. Surface plasmon (polaritons) resonances (SPR) result from the hybridization of the bulk plasmons with free-space radiation, which takes place at the interface of the plasmonic material and a dielectric medium. Along with the nature of the conducting material, the dielectric

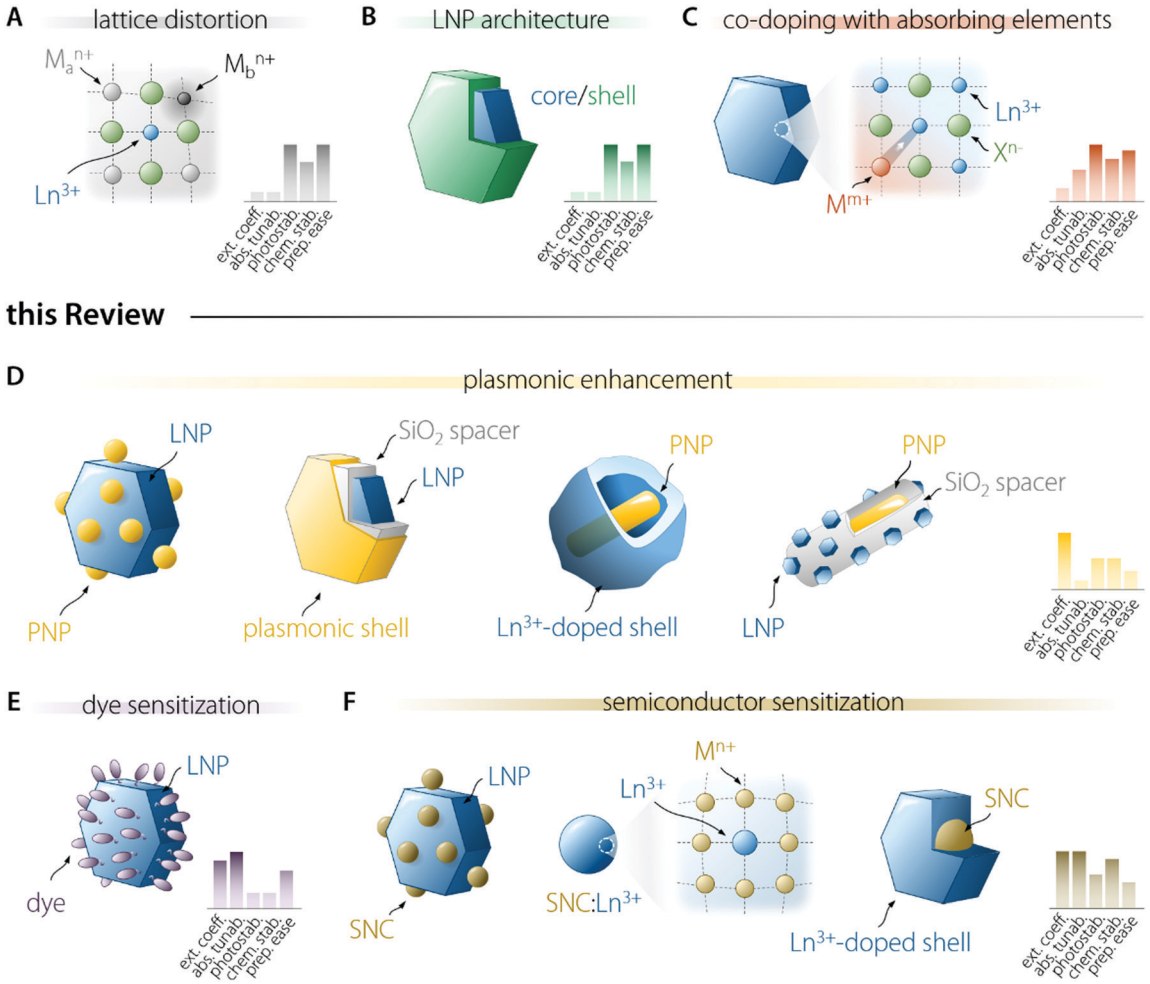

Fig. 2 Graphical summary of the strategies employed for the enhancement of Ln^{3+} emission brightness. (A) The modification of the lattice by the incorporation of defects and lattice-distorting ions effectively lowers the coordination symmetry of Ln^{3+}, ultimately leading to a relaxation of the parity rule for intraconfigurational f–f transitions. (B) Preparation of LNPs with multi-shell architecture, where different Ln^{3+} ions are spatially confined and protected from quenchers (*e.g.*, solvent molecules with high-energy vibrations) allows minimizing energy losses, thus yielding brighter Ln^{3+} emission. (C) Co-doping with Ln^{3+} and ions featuring allowed electronic transitions (Ce^{3+}, Bi^{3+}...) is a viable strategy to enhance the light absorbing capability of LNPs. These approaches (A–C), albeit easy realized, theoretically afford a limited enhancement of the LNP capability to absorb the excitation light. For this reason, in this review we focus on three other approaches that can theoretically grant brighter Ln^{3+} luminescence. (D) Plasmon-enhancement entails the use of moieties featuring localized surface plasmon resonance (LSPR), which can improve both the absorption and emission efficiency of the coupled LNP. (E, F) Dyes and semiconductors can both be used as excitation light harvesters and, upon proper coupling/amalgamation with LNPs, they can transfer the absorbed energy to Ln^{3+}. These three latter strategies promise the highest absorption enhancement and tunability but the synthesis of these nanosystems require a higher degree of finesse.

constant of the medium determines the oscillation frequency of the charge carriers. When the carriers are spatially confined, as is the case for plasmonic nanoparticles (PNP), the natural frequency of these collective oscillations also depends on the size and geometry of the PNP. This is referred to as localized surface plasmon resonance (LSPR) and is the phenomenon of interest in the current frame. In fact, although there are numerous examples of UC emission enhancement using patterned plasmonic surfaces and 2D structures,[33,34] we are herein focusing only on colloidal systems. Clearly, for preparing such systems, PNPs ought to be used.

The enhancement of Ln^{3+} emission stems from the influence of surface plasmons on three distinct parameters, which synergistically contribute to determining the overall emission brightness: decay rates (*i.e.*, radiative and non-radiative relaxations), energy transfer coefficients, and absorption cross-section.[35] We should note here that albeit the focus of this review is the betterment of the absorption capability of the LNPs, to comprehensively address the topic of plasmon-enhanced emission, we also discuss the cases wherein increased radiative decay rate plays a major role. Indeed, often the effects cannot be completely disentangled and other times the explanation offered by the authors for the observed emission enhancement is more an "educated guess" than a definitive explanation.

An in-depth discussion of the fundamentals of each aspect lies beyond the scope of this manuscript and the interested reader is encouraged to read the instructive review from Park *et al.*[35] For the sake of the present discussion, it is sufficient to

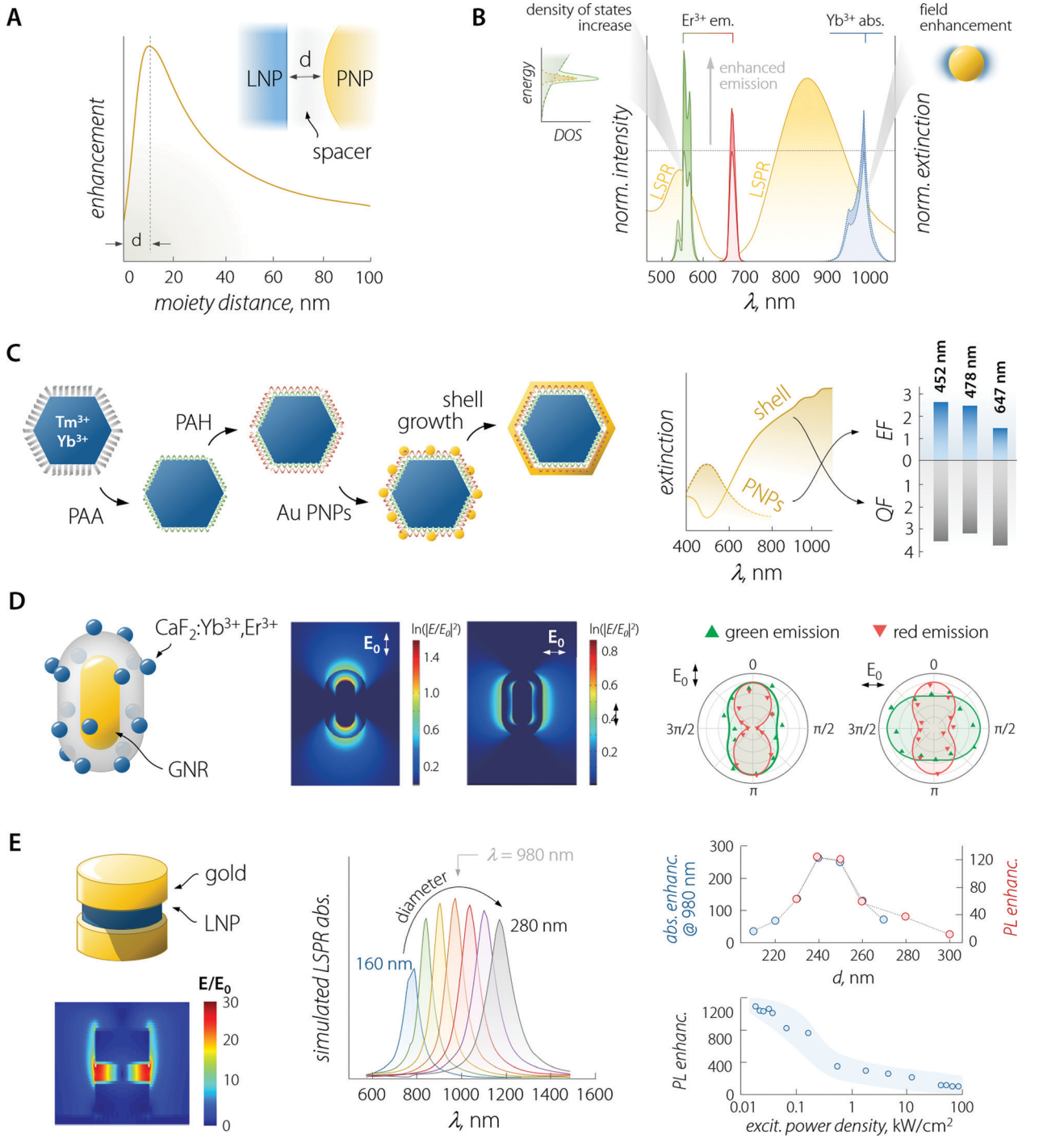

Fig. 3 Plasmon-enhanced LNP emission. (A) The enhancement factor is a complex function of the PNP–LNP separation distance with its maximum falling at a value determined by several effects discussed in the main text. (B) Plasmon-enhancement in a Yb^{3+}/Er^{3+} upconversion system, where absorption (due to local field enhancement) and emission (due to the Purcell effect) are simultaneously achieved. (C) Scheme of sequential decoration of Yb^{3+}/Tm^{3+}-doped LNP with gold nanospheres and the complete coverage with a gold nanoshell, along with the extinction spectra and enhancement/quenching factors observed for the two architectures. Adapted with permission from ref. 53. Copyright 2010 Wiley-VCH. (D) Decoration of a single SiO_2-coated GNR with CaF_2-based small LNPs. Local field enhancement under 980 nm excitation varies considerably in intensity and spatial distribution, depending on the relative orientation of the impinging light (E_0) and the GNR. The different behaviour of the observed polarization of green and red emitted light arises mainly from the coupling between LSPR and UC emission rather than from laser polarization. Adapted with permission from ref. 39. Copyright 2016 Springer-Nature. (E) In a structure comprised of LNPs sandwiched between gold nanodisks, the field (980 nm) is greatly enhanced within the LNPs. Moreover, the position of the LSPR peak of the structure can be tuned by varying the diameter of the plasmonic moieties (gold disks above and below the LNP). In reality, the produced structures have an upper disk smaller than the lower one (approx. 85%). The simulated absorption (blue) and overall measured PL (red); enhancement is found with a diameter of the lower gold disk between 240 and 250 nm, yielding a maximum enhancement of >1000 at low excitation powers. Adapted from ref. 52.

say that (i) absorption is mainly influenced by the local field enhancement, (ii) radiative decay rate is enhanced by the increased photon density of the states (Purcell effect), (iii) non-radiative relaxation is impacted by ohmic losses induced by the presence of metal, (iv) experimental reports indicate that energy transfer enhancement is generally observed for systems with large donor–acceptor separation distance and as such featuring intrinsically inefficient transfer. Regarding the last point, in the case of LNPs, the donor–acceptor distance refers to the separation between the sensitizer and activator ions in the particle lattice. Considering the large amount of sensitizers introduced in LNPs (often between 20 and ~100%),[36] the average distance between the neighbouring ions is short, making the energy transfer between them efficient enough so that its further enhancement using plasmonic moieties is difficult to achieve.[37] Importantly, the interplay between the first three points yields an emission enhancement factor whose maximum falls at a specific separating distance between LNP and PNP.[38] This distance defines the optimal thickness of the spacer between the two moieties (Fig. 3A – generally of the order of 10 to few tens of nanometres). In the case of LNP–PNP coupling, such a spacer is often made of silica;[38–42] however, polymers have also been used.[43,44] Another important aspect to consider is that larger PNPs always feature stronger scattering of light, which induces higher luminescence enhancement compared to their smaller counterpart.[45,46] For smaller particles, the LSPR peak overlaps with the emission support instead of a more efficient quenching of the luminescence *via* energy transfer (likely due to their dominant absorption over scattering).[47] This is a pivotal consideration, which provides further guidelines for the design of the most suitable plasmonic system for plasmon-enhanced luminescence.

Considering the observations above, the enhancement of LNP emission can be achieved by simultaneously matching the excitation and/or the emission wavelengths, thus exploiting the absorption enhancement and the radiative decay rate increase, respectively (Fig. 3B).[48,49] This was also demonstrated in dye molecules coupled to individual silver nanoprisms.[50] Regarding LNPs in particular, it is important to note that while plasmon-induced enhancement of downshifting emission has a quadratic dependence on the local field enhancement, the anti-Stokes process of UC depends on the fourth power of this parameter.[35,51] It therefore comes as no surprise that studies on plasmon-enhanced UC are far more common than studies on downshifting enhancement, also because emission processes that are intrinsically poorly efficient (such as UC) are more easily enhanced harnessing plasmonic effects. Nonetheless, we should point out that UC is a process that relies on the long-lived nature of the Ln^{3+} energy states for the successive absorption of photons. Therefore, any increase in the decay rate of an intermediate energy state involved in the population of higher-energy levels is detrimental to this anti-Stokes optical process. A fitting example is offered by a Yb^{3+}–Er^{3+} co-doped material, where the excitation of Yb^{3+} at 980 nm fosters UC emission of Er^{3+}. In some instances, it has been observed that a perfect match between LSPR and Yb^{3+} absorption was not the most favourable situation for plasmon-enhancement.[52] A wavelength mismatch instead allowed the maximization of the optical performance of the combined system, likely due to a less pronounced lifetime shortening (*i.e.*, decay rate increase) of the Yb^{3+} $^4F_{5/2}$ excited level that happens in particular for zero-phonon transitions.

Lastly, a point should be made regarding the versatility of plasmon enhancement as a strategy. The position of the LSPR peak featured by the PNPs can be controlled by several means such as the nature of the plasmonic material, size and morphology, as well as the presence of interfaces with different materials are all parameters that can be harnessed to fine-tune the LSPR position. Gold is the most versatile material for the preparation of PNPs and decades of experience have produced a vast literature of synthetic approaches. Nanospheres, nanorods (GNRs), nanoshells (GNSs), and nanourchins are only some of the proposed gold-based PNPs, and their LSPR covers a wide gamut of wavelengths, from visible to the second biological window (NIR-II, 1000–1350 nm). Silver is another noble metal with suitable plasmonic properties but also some oxides (indium tin oxide – ITO,[54] W_xO[55]), chalcogenides (Cu_xS, Cu_xSe),[56] and boride (LaB_6)[57] nanoparticles feature LSPR. For many of these latter PNPs, plasmonic resonance can be easily extended in the near-infrared (NIR) beyond 1000 nm, whereas PNPs based on noble metals tend to have their LSPR in the visible (unless cumbersome or high aspect-ratio systems are prepared). Despite this flexibility in terms of the tuning of the optical properties, the coupling of PNP with LNP does not afford broadband excitability. Indeed, the excitation wavelength is still determined by the Ln^{3+} whose absorption is to be enhanced.

In the rest of this section, we discuss selected examples of the plasmonic enhancement of LNP emission (Table 1), subdividing the approaches depending on the architecture of the final system. As mentioned above, most of the examples deal with UCNPs.

3.1.1. Decoration of LNP with PNPs. One of the most straightforward approaches explored for the plasmonic manipulation of LNPs' emission is their decoration with PNPs. This method is generally accomplished with gold and silver NPs, whose LSPR peak falls predominantly in the visible part of the electromagnetic spectrum. This allows harnessing the Purcell effect to enhance the UC emission.[58] However, above 100 nm in size, the extinction spectrum of gold NPs extends more decisively in the NIR. In that vein, it was observed by Fischer *et al.* that larger gold NPs are better suited for enhancing Er^{3+} emission at 980 nm under 1520 nm excitation due to increased scattering by large structures.[45] When it comes to colloidal systems, both enhancement and quenching of the emission were observed in LNPs decorated with PNPs. To that end, silver PNPs (λ_{LSPR} = 415 nm) were used to enhance the emission of $NaYF_4$:Nd^{3+},Yb^{3+},Ho^{3+} LNPs.[59] The authors found that a 10 nm thick SiO_2 spacing layer afforded the largest enhancement factors (15 and 7.5 for green and red emission, respectively) both under 808 and 980 nm excitation in cyclohexane. The enhancement followed from the increase in the radiative decay rate (Purcell effect) rather than from absorption enhancement, as also expected from the lack of overlap between LSPR and the excitation light. These results were consistent with those obtained for $NaYF_4$:Yb^{3+},Er^{3+} LNPs combined with 15 nm silver PNPs.[42] Duan, Huang, and co-workers

Table 1 Summary of the main parameters describing the properties of most relevant LNPs featuring plasmon-enhanced emission described in Section 3.1

Ln^{3+}-Doped material	Plasmonic material	Spacer	Structure	Excitation wavelength (nm)	Highest enhancement factor (emission range)	Ref.
$NaYF_4$:Nd^{3+},Yb^{3+},Ho^{3+}	Ag nanospheres	SiO_2	LNP/SiO_2/PNPs	808, 980	15 (green), 7.5 (red)	59
$NaYF_4$:Yb^{3+},Er^{3+}	Ag nanospheres	SiO_2	LNP/SiO_2/PNPs	980	14.4 (green), 12.2 (red)	42
$NaYF_4$:Yb^{3+},Tm^{3+}	Au nanospheres, Au shells	PAA–PAH	LNP/polymer/PNPs, LNP/polymer/shell	980	Nanospheres: 2.5 (blue), 1.5 (red) shell: <1 (blue, red)	53
Na(Y,Gd)F_4:Yb^{3+},Er^{3+},Tm^{3+}	Ag nanospheres	SiO_2	LNP/SiO_2/PNPs	980	3–4 (green, red, NIR)	60
$NaYF_4$:Yb^{3+},Tm^{3+}	Au NRs	PMAM	LNP/PMAM/NRs	980	Shorter NRs: 11.2 (visible) longer NRs: 27 (NIR)	43
$Ce_{0.9}Tb_{0.1}F_3$ and LaF_3:Yb^{3+},Er^{3+}	Au NRs	SiO_2	NR/SiO_2/Ln^{3+}-disks	255, 980	$Ce_{0.9}Tb_{0.1}F_3$:2.3, 3.7, 1.9, 1.8 (Tb^{3+}:$^5D_4 \rightarrow {}^7F_{6,5,4,3}$) LaF_3:Yb^{3+},Er^{3+}: 6.5 (green), 6.2 (red)	67
$NaGdF_4$:Yb^{3+},Nd^{3+}/$NaGdF_4$:Yb^{3+},Er^{3+}/$NaGdF_4$	Au NRs	SiO_2	NR/SiO_2/LNPs	808, 980	2 (blue), 20 (green), 8 (red)	49
CaF_2:Yb^{3+},Er^{3+}	Au NRs	SiO_2	NR/SiO_2/LNPs	980	3 (green), 6.7 (red)	39
$NaYF_4$:Yb^{3+},Tm^{3+} (or Er^{3+})	Au shell	Citrate	LNP/shell	975	Tm^{3+}: 5.5 (blue), 8.5 (red), 4.5 (NIR)	68
$NaYF_4$:Yb^{3+},Er^{3+}	Au shell	SiO_2	LNP/SiO_2/shell	980	3.3 (blue), 2.5 (green), 2.2 (red)	69
$NaYF_4$:Yb^{3+},Er^{3+},Tm^{3+}	Au and Ag shells	PMAM	LNP/PMAM/shell	980	Ag: 20 (blue), 3 (green, red) Au: 2.3 (blue), 20 (green)	44
Y_2O_3:Er^{3+}	Ag nanospheres	SiO_2	PNP/SiO_2/Ln^{3+}-shell	980	4 (green + red)	72
Y_2O_3:Yb^{3+},Er^{3+}	Au nanospheres	SiO_2	PNP/SiO_2/Ln^{3+}-shell	980	9.59 (green), <1 (red)	73
Lu_2O_3:Gd^{3+},Yb^{3+},Er^{3+}	Ag nanospheres	SiO_2	PNP/SiO_2/Ln^{3+}-shell	980	30 (green + red)	71
$NaYF_4$/$NaYF_4$:Yb^{3+},Er^3	$Cu_{1.8}S$	—	PNP/Ln^{3+}-shell	980	6.9 (green), 7.5 (red)	79
Nd_2O_3	Au NRs	—	NR/Ln^{3+}-shell (rattle-like)	730	4.6 (870 nm)	74
$NaYF_4$:Yb^{3+},Er^{3+}	Au disks	—	Disk/LNP/disk (sandwich)	980	>1000 (green)	52
Y_2O_3:Yb^{3+},Er^{3+}	Au cap	—	Ln^{3+}-sphere/cap	980	64 (green), 101 (red)	80
$NaYF_4$:Yb^{3+},Er^{3+}	Au cap	—	Ln^{3+}-NR/cap	980	>100 (green, red)	81

compared the effect of sub-micrometric LNP decoration with gold PNPs and the growth of a continuous gold shell (Fig. 3C).[53] LNPs were successively decorated with polyacrylic acid (PAA) and polyallylamine hydrochloride (PAH), exploiting the negative and positive charge, respectively, featured by the two polymers. Gold PNPs (seeds) were then attached to the surface of the LNPs (made of $NaYF_4$:Yb^{3+},Tm^{3+}) and their coalescence was induced by the addition of gold precursor in the suspension, yielding a continuous metal shell. The enhancement of Tm^{3+} emission (452, 478, and 647 nm) was observed only in the presence of PNPs with absorption in the visible range, while quenching was induced by the metal nanoshell. This last effect was ascribed to the scattering of the excitation light (owing to the NIR-centred LSPR of the shell), yielding a lower overall excitation light flux and to the reduced transmission of UC emission through the shell. Xing *et al.* prepared a sub-50 nm system comprising Na(Y,Gd)F_4:Yb^{3+},Er^{3+},Tm^{3+}/SiO_2/gold nanospheres.[60] Several UC emission lines stemming from Er^{3+} and Tm^{3+} were observed between 500 and 800 nm, while the gold PNPs featured an extinction stretching throughout the whole visible range. Upon the optimization of the spacer thickness (10–15 nm) and PNPs amount, a 3/4-fold enhancement of UC emission was achieved. The brighter luminescence allowed for *in vitro* and *in vivo* visualization of the particles under 980 nm excitation, while the magnetic and X-ray absorption properties of Ln^{3+} also endowed the system with MRI and computed tomography imaging capabilities. Similarly, Jiang *et al.* demonstrated an almost 80-fold enhancement of Gd^{3+} UC emission in $NaYF_4$:Gd^{3+},Yb^{3+},Tm^{3+} by carefully controllying the total amount of attached small gold PNPs.[61] One limitation of the approaches discussed above is that the spectral overlap between LSPR and LNP emission could also induce absorption of the emitted light by the PNPs. This scenario is most detrimental for the increment of the brightness of LNPs but it can be harnessed for bioassays and colour-tuning.[41,62–65]

The enhancement of UC luminescence was also observed in GNR-decorated $NaYF_4$:Yb^{3+},Tm^{3+} LNPs.[43] A polyamidoamine dendrimer was used to functionalize the surface of LNPs, and GNRs were grown *in situ* on the surface of the structure. The extinction spectrum of GNRs was characterized by two contributions at 520 and 805 nm owing to the LSPR transverse ad longitudinal modes, respectively. On extending the GNR growth time to 240 min, the light extinction efficiency of the plasmonic particles increased, resulting in a maximum 27-fold enhancement of NIR-to-NIR UC luminescence (Tm^{3+} emission at 800 nm) under 980 nm excitation. At shorter growth times, the GNRs had a smaller aspect ratio, which resulted in the preferential improvement of the UC visible emission (11.2-fold) compared to NIR. The nanocomposite (GNRs + LNP) functionalized with 2-thiouracil was employed by the authors for uric acid (UA) sensing: in the presence of UA, the particles aggregated, yielding changes in both the extinction and luminescence spectra. Both signals could be used to determine the UA concentration with a detection limit as low as 1 pM.

3.1.2. Decoration of PNP with LNPs. In recent years, this approach has been extensively exploited by several researchers. The most common structure is a single high-aspect ratio PNP (or a pair of them[66]) coated with a silica layer of controlled thickness (spacer), on top of which several small LNPs are attached (Fig. 3D).[39,49,67] Simultaneous excitation and emission enhancement were achieved by Kang *et al.* using engineered core/shell/shell LNP to decorate the surface of a 25 × 80 nm GNR coated with a 28-nm thick mesoporous SiO_2 layer.[49] The transverse

LSPR was centred in the green region, while the longitudinal mode fell in the NIR, encompassing both 808 and 980 nm (*i.e.*, the excitation wavelengths used for Nd^{3+} and Yb^{3+} excitation, respectively). It is interesting to note that studies for the plasmonic enhancement of LNP emission generally make use of rather simple LNP architectures, while in the mentioned study, the segregation of sensitizers (Nd^{3+}, Yb^{3+}) and activator (Er^{3+}) in different LNP regions, along with the growth of a passive shell were performed. Overall, an enhancement factor of 20 was achieved for green emission (upon 808 nm excitation), whose lifetime was substantially shortened due to the Purcell effect (and possibly due to the introduction of other non-radiative decay pathways). A similar system was prepared by He *et al.*, who employed CaF_2:Yb^{3+},Er^{3+} LNPs tethered to the surface of SiO_2-coated GNRs (Fig. 3D).[39] The authors observed enhanced green and red UC emission owing to the spectral overlap of these emission lines with the transverse and longitudinal LSPR modes of the GNR. Even more interestingly, it was verified that the emitted light was strongly polarized. While the polarization of red emission did not show correlation with the relative orientation of the GNR axis and the polarization direction of the excitation light (E_0), green UC emission appeared to be dependent on this parameter. This behaviour stemmed from the stronger contribution to the overall emission coming from the LNPs located at the tips or at the sides of the GNR when E_0 is parallel or perpendicular to the GNR's axis, respectively. Indeed, while red UC emission remained polarized along the GNR axis, irrespective of the excitation light orientation and LNP location, these two parameters strongly influenced the polarization of the green UC emission. By performing electrodynamic calculations within the frame of FRET theory, the authors could unravel complex interactions underpinning this behaviour. In particular, the relative orientation and degree of interaction between the emission dipoles in the LNPs and the transverse/longitudinal plasmonic dipoles within the GNR were shown to play a key role.

3.1.3. Growth of plasmonic shells on LNPs. Considering gold-based plasmonic nanostructures, an effective way to push their LSPR within the NIR (thus matching the absorption of typical Ln^{3+} used as sensitizers, such as Nd^{3+} and Yb^{3+}) is the preparation of nanoshells. These are structures of few nanometres in thickness grown on top of a dielectric core, such as silica particles. The tuning of the ratio between the SiO_2 core size and metal thickness allows controlling the position of the LSPR peak. SiO_2-coated LNPs covered with a layer of noble metal are indeed among the most explored structures in this context, although the growth of a gold shell directly on LNP has also been performed. In this vein, we mentioned in Section 3.1.1 a study from Duan, Huang, and co-workers, wherein a gold shell was grown atop the LNPs. As opposed to the decoration with PNPs, the gold shell induced the quenching of $NaYF_4$:Yb^{3+},Tm^{3+} emission (Fig. 3C).[53] However, the enhancement of LNP emission with plasmonic shells was achieved in other studies. For example, the direct growth of a gold shell on citrate-functionalized cubic α-$NaYF_4$:Yb^{3+},Er^{3+} (or Tm^{3+}) NPs afforded UC emission intensity comparable to that exhibited by the same material in the hexagonal (β) polymorph.[68] Priyam *et al.* controlled the thickness of the gold shell grown on SiO_2-coated $NaYF_4$:Yb^{3+},Er^{3+} LNPs, thus effectively tuning the LSPR peak maximum from 580 to 900 nm.[69] The thinner the shell, the more red-shifted the extinction. Enhancement was observed only in the case of 900 nm-centred LSPR, thanks to the highest extinction at 980 nm (*i.e.*, the LNP excitation wavelength) and reduced LSPR overlap with the Er^{3+} emission lines centered at 410, 550, and 660 nm. All the other tested LNP/SiO_2/GNSs instead showed quenched UC emission. The optimized nanostructure was used for simultaneous fluorescence and dark field imaging of the B16-F0 cells, leveraging the light scattering of GNS for the latter imaging modality. Kannan *et al.* instead explored a silica-free approach, where the LNPs were modified with a polyamidoamine dendrimer of first generation (PMAM G1).[44] The polymer offered a suitable substrate over which gold or silver shells were grown, yielding increased green or UV-blue UC emission enhancement, respectively.

3.1.4. Growth of Ln^{3+}-doped shells on PNPs. A strategy complementary to the one discussed above involves the growth of a Ln^{3+}-containing shell on PNPs. Different approaches have been explored, such as the growth of the Ln^{3+}-doped shell directly on the surface of the plasmonic particles,[70] the use of a spacer between the two species,[40,71–73] as well as the selective etching of a silica spacer to achieve rattle-like structures.[72,74] Stucky and co-workers grew a Y_2O_3:Er^{3+} shell onto SiO_2-coated silver NPs,[72] adapting a strategy for the preparation of rare-earth nanostructures with urea and rare-earth salts.[75] Optimal spacer thickness was found to fall between 20 and 40 nm, depending on the diameter of the silver NPs (from 20 to 130 nm). An analogous structure was prepared by replacing Ag NPs with Au NPs; a spacer thickness of 40 nm afforded an almost 10-fold enhancement of green Er^{3+} emission thanks to the overlap of the LSPR peak (centred at 527 nm) with Er^{3+} emission.[73] A shell of Lu_2O_3:Gd^{3+},Yb^{3+},Er^{3+} was also grown on the SiO_2-coated Ag NPs using the same approach.[71] The resulting nanosystem was used as a probe for the fluorescence imaging of HeLa cells and featured a 30-fold enhancement in the luminescence compared to the control sample lacking PNPs. Interestingly, similar structures with GNRs coated with Ln^{3+}-doped fluoride[76,77] or oxyfluoride[78] shells showed quenched UC emission. Recently, the first example of plasmonic-enhancement of the UC luminescence of colloidal LNPs using non-metal-based PNPs was reported. $Cu_{1.8}S$ nanoparticles were coated with two shells of $NaYF_4$ doped respectively with Yb^{3+} and Yb^{3+}–Er^{3+}.[79] The authors claimed that the NIR-centred LSPR of the chalcogenide PNPs, along with the optimization of the Yb^{3+} content in the intermediate layer (30%), afforded a maximum of 28-fold and 101-fold enhancement of green and red UC emission, respectively, thanks to the enhancement of the absorption capability of the system. However, we note that these numbers were obtained by comparing the emission of $Cu_{1.8}S$/$NaYF_4$:Yb^{3+}(30%)/$NaYF_4$:Yb^{3+},Er^{3+} and the reference LNPs of $NaYF_4$/$NaYF_4$:Yb^{3+},Er^{3+} (the latter lacking Yb^{3+} in the core). It is thus very possible that a substantial part of the enhancement stemmed from an increased number of sensitizer ions capable of absorbing the excitation light (980 nm) in the intermediate shell rather than from

plasmonic enhancement. A more conservative 6.9- and 7.5-fold increase, obtained by comparing the same LNPs with $Cu_{1.8}S$/$NaYF_4$/$NaYF_4$:Yb^{3+},Er^{3+}, thus seems more reasonable. Lastly, moving from UC, the enhancement of Nd^{3+} downshifting emission was achieved in the GNR/Nd_2O_3 nanocomposites.[74] The structure was prepared *via* a hydrothermal method at relatively low temperature (85 °C) and the tuning of LSPR allowed to reach a maximum enhancement factor of approximately 4.6 for Nd^{3+} emission at 873 nm under 730 nm excitation.

3.1.5. Other structures. Aside from the appearance of extended polaritons in periodic structures, the reason why patterned surfaces are often used for the enhancement of the luminescence has to be searched in the non-isotropic nature of the electromagnetic field enhancement.[82] In fact, on surfaces, it is possible to control the relative disposition and orientation of the plasmonic antennas and LNPs. The confinement of the enhanced field in selected regions and careful positioning of the LNPs therein affords unrivalled plasmon-mediated sensitization. Clearly, control over the relative spatial orientation of LNP and PNP is pivotal in a colloidal system. Unfortunately, this directionality is not easily achieved with classical wet chemistry methods. To that end, recently the group of Park reported on the combination of wet chemistry (for UCNP synthesis) and lithography (for the growth of the metal moiety);[52] this hybrid method affords nanostructures where LNPs are sandwiched between two gold plasmonic layers (Fig. 3E). This architecture maximizes the field enhancement within the LNP and the LSPR peak could be tuned to match Yb^{3+} absorption by controlling the diameter of the sandwiching plasmonic disks. Due to the experimental limitations, a mismatch of approximately 85% was observed between the upper and lower gold disks, leading to a slight deviation from the plasmonic behaviour modelled for the case of perfectly identical metal moieties. These structures show above 1000-fold luminescence enhancement at low excitation power density and approximately 100-fold at high powers. Such an enhancement was measured while the nanocomposite was still attached to the silicon substrate used for lithography. In fact, a smaller 50-fold luminescence enhancement was observed at a high-power density for the nanocomposite when dispersed in water. Another interesting example is provided by the study of Fujii and co-workers, who combined wet-chemistry and thermal evaporation to prepare Y_2O_3:Yb^{3+},Er^{3+} nanoparticles with a gold cap.[80] To prepare this structure, the nanoparticles were deposited on a fuse quartz substrate, covered with a Ti adhesion layer and finally, gold deposition was accomplished at a controlled angle from the normal to the substrate. The nanostructures were then dispersed in polydimethoxysilane resin. Varying the gold deposition angle, the cap shape was tuned and, consequently, its plasmon resonance. When the LSPR approached 980 nm (Yb^{3+} absorption), the authors found maximum green and red UC emission enhancement of 64 and 101, respectively. The authors further expanded on this topic, achieving the coating of $NaYF_4$:Yb^{3+},Er^{3+} nanorods with gold caps using the same approach.[81] Also in that case, the emission brightness increased capitalizing on more efficient light absorption of the nanocomposite.

3.2. Organic antennas

Together with the use of semiconductors, this approach grants broadband sensitization of LNP emission, which is in stark contrast with the spectrally narrow absorption lines intrinsically featured by lanthanide ions. The organic sensitization of LNPs typically involves the use of organic dye molecules anchored on the inorganic LNP surface to implement the antenna effect.[83] Frequently, the authors describe the effect of the dye as "brightness enhancement". Although an increased brightness is indeed the ultimate effect, the direct consequence of dye attachment/decoration is an enhancement of the absorption properties of the Ln^{3+}-doped nanoparticle. This attachment of the organic dyes on the surface of the LNPs can proceed through the routes of covalent bonding, electrostatic attraction, physical absorption, or their combination.

Upon electromagnetic irradiation, the dye molecule is promoted to its excited singlet electronic state(s). Subsequently, de-excitation takes place through several processes (Fig. 4A), such as:

– Non-radiative internal conversion (IC) at the dye molecule.

– Intersystem crossing (ISC) between singlet and triplet state of such molecules.

– Fluorescence emission (E).

– Energy transfer (ET) from the dye molecule acting as a donor to Ln^{3+} (mostly on the surface of the LNP) as an acceptor. It involves the relaxation of dye molecules to the ground state, together with the promotion of Ln^{3+} to their excited state.

Zooming into a more detailed description of the fourth step, it typically proceeds through either Förster or Dexter non-radiative energy transfer or a combination of the two.

For a given donor–acceptor pair (Fig. 4B), (i) the Dexter mechanism is an exchange interaction, which involves double electron transfer and requires a sizeable orbital overlap between the wavefunctions of organic molecules as the donor (D) and the Ln^{3+} as the acceptor (A); (ii) Förster (or dipole–dipole) mechanism is an electrostatic interaction, in which the dipole moment associated with the dye molecule's state couples with the dipole moment of the 4f orbitals. In addition, dipole–multipole transfers play a non-negligible role in the sensitization of Ln^{3+} ions.[84,85]

Both singlet and triplet states of the organic molecules may transfer energy to the lanthanide ion, possibly with the assistance of phonons. However, since the singlet state is short-lived, transfer from this latter level is often not efficient. The most likely energy transfer process to happen (ET from S_1; Fig. 4A) leads as its outcome to the relaxation of dye molecules to the ground state S_0 and promotion of Ln^{3+} to an excited state. But it is also possible that ISC (whose likeliness is inversely proportional to the S_1–T_1 energy gap) can occur more efficiently than the ET from S_1 just described. If that is the case, the dye molecule will first switch to its triplet state (T_1), then an ET from T_1 to Ln^{3+} may happen. This second kind (and less likely to occur) ET can be Förster, Dexter, or both simultaneously. In a majority of the published dye–Ln^{3+} systems, emphasis has been put on Förster-based description only because of the higher ET rate from S_1 over the ISC one. Inter-distance wise, at an estimated dye molecule–Ln^{3+} distance in the

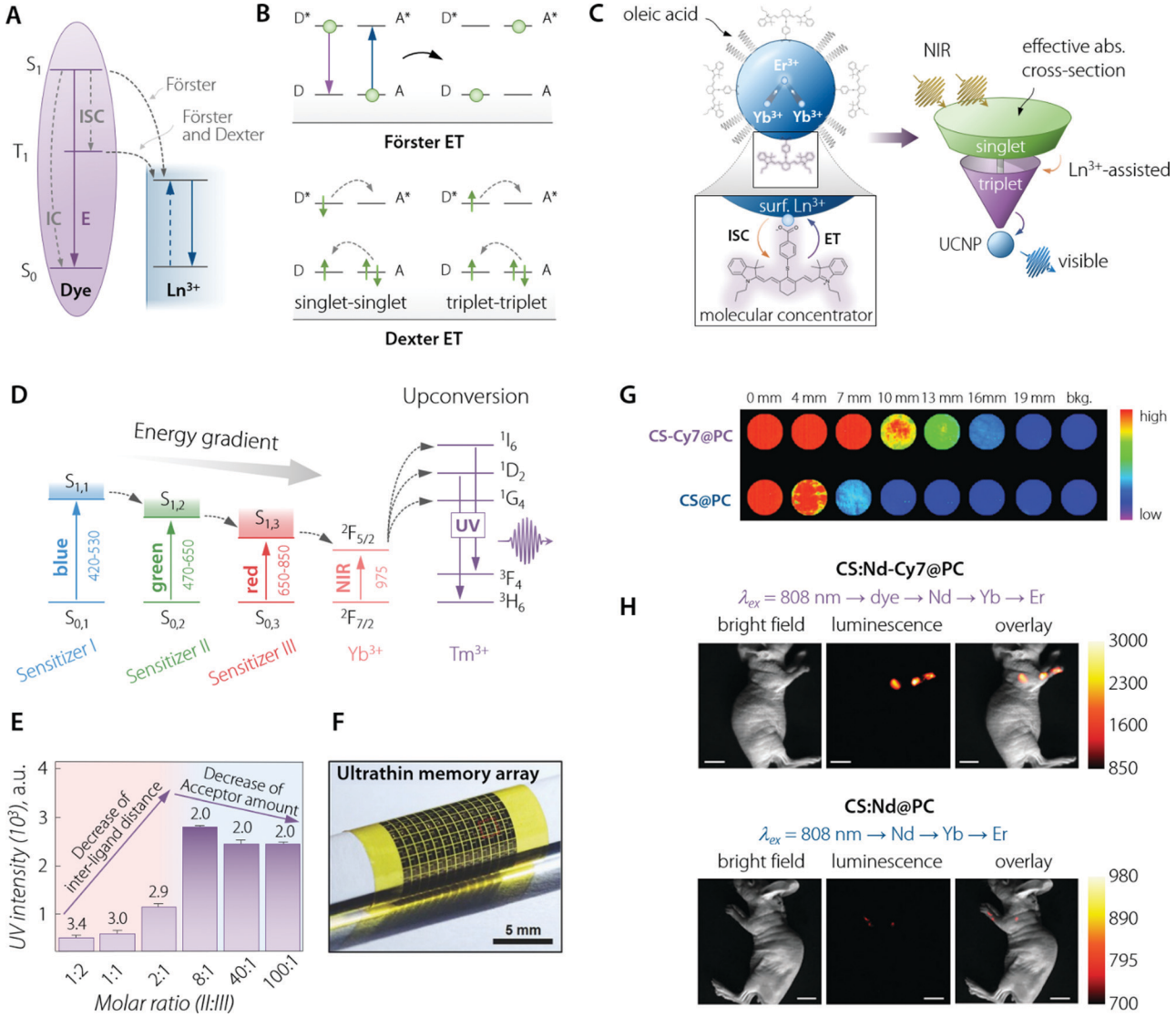

Fig. 4 Organic (dye) antenna. (A) Schematic of the energy transfer mechanisms, Förster and Dexter. (B) Schematic illustration of non-radiative energy transfer processes from the dye to Ln^{3+}. E, IC, and ISC represent the luminescence emission, internal conversion, and intersystem crossing, respectively. Adapted with permission from ref. 89. Copyright 2017 Royal Society of Chemistry. (C) (top left) Cartoon schematic of the dye-sensitized UCNP system, showing IR-806 bound to the UCNP surface (not to scale), and an upconversion event inside the UCNP where two excited Yb^{3+} non-radiatively and sequentially excite Er^{3+} into a higher energy state. (bottom left) Magnified illustration of the interactions between IR-806 and a surface lanthanide—the heavy nucleus of the lanthanide aids in ISC from IR-806 $S_1 \rightarrow T_1$ states, allowing much more efficient T_1 sensitization of the Ln^{3+} ions within the UCNP. (right) Depiction of the antenna-like nature of IR-806 in sensitizing the UCNP, conveying the much larger absorption cross-section of IR-806 relative to the UCNP, as well as $S_1 \rightarrow T_1$ ISC enhancement by Ln^{3+}. Adapted with permission from ref. 86. Copyright 2018 Springer-Nature. (D) Energy diagram of a three sensitizer-system and ions of the so-sensitized UCNPs. The thick horizontal lines represent the energy levels and the arrows represent the sequential energy transfer. (E) Upconverted UV emission intensity from the double-ligand UCNPs (1.6 mg mL^{-1}). Molar ratios of sensitizer II and III range from 1 : 2 to 100 : 1. The 517 nm laser power density is 25 mW mm^{-2}. The number written above the purple bars indicates the calculated interligand distances (nm). Overall, the figure shows that there is a trade-off (appreciable in terms of final UV emitted intensity) between the increasing number of sensitizer ligands and the relative decrease in the acceptor amount. That is, the former effect is beneficial for absorption of the excitation beam while the latter decreases the effective transfer of optical energy to Tm^{3+} ions. (F) Image of the integrated device array on a flexible plastic substrate. (F, G, and H) are adapted with permission from ref. 90. Copyright 2017 Wiley. (G) NIR imaging of CS & Cy7@PC and CS@PC through the pork tissue of varied thickness (excited at 800 nm). Adapted with permission from ref. 91. Copyright 2018 Royal Society of Chemistry. (H) UC luminescence lymphatic imaging at 30 min post injection of (upper) CS:Nd-Cy7@PC and (bottom) CS:Nd@PC under irradiation at 808 nm ($\lambda_{UCLumin}$ = 540 ± 12 nm, scale bar = 10 mm). Adapted with permission from ref. 92. Copyright 2016 Royal Society of Chemistry.

1–2 nm range, Dexter ET was usually found to be negligible or, at maximum, comparable with the Förster mechanism.

Albeit a selected list of representative applications and developments of the organic antenna approach for the enhancement of LNPs absorption is included within this section (Table 2), we decided to highlight here the innovative work by D. J. Garfield *et al.*[86] Therein, the authors managed to amplify UC nanoparticles' (UCNPs) emission by enriching the molecular antenna

Table 2 Summary of the main parameters describing the properties of most relevant LNPs featuring dye-sensitized emission described in Section 3.2

LNP	Dye molecule	Excitation wavelength (nm)	Enhancement (emission range)	Ref.
β-NaY^{3+} $(78 - x)$%$Gd^{3+}$$x$%$Yb^{3+}$ 20%Er^{3+}20%F_4	IR-806	808	33 000-fold (520 to 680 nm; Er^{3+} VIS emission)	86
Y^{3+}80%Ln^{3+}20%F_4 (Ln = Nd^{3+} or Yb^{3+})	Tropolonate (Trop)	340	Not reported (900–1100 nm) luminescence lifetimes (longest components) >5 times longer (Yb) >11 times longer (Nd)	93
La^{3+}95%Eu^{3+}5%F_3	6-Carboxy-50-methyl-2,20-bipyridine ($bipyCOO^-$)	305	~100-fold (615 nm)	94
β-$NaYF_4$:Yb^{3+},Er^{3+}	IR-806	800	3300-fold (720–1000 nm)	95
($NaYbF_4$:Tm^{3+} 0.5%)/$NaYF_4$:Nd^{3+}	IR-808	800	14-fold (300–700 nm; Tm^{3+} UC range)	96
$NaYF_4$:Tm^{3+},Yb/$NaYF_4$:Yb^{3+}	IR-1061	980	2.8-fold (800 nm)	97
$NaYF_4$:Yb10%,Er2%/$NaYF_4$: Nd 30%	IR-783	670–860	Not reported (300–700 nm)	98
$NaYF_4$:Yb^{3+},X/$NaYbF_4$/$NaYF_4$:Nd^{3+} (X = null, Er^{3+}, Ho^{3+}, Tm^{3+}, or Pr)	Indocyanine green (ICG)	700–860	4-fold (multipeak between 1000–1600 nm)	99
β-$NaYF_4$:Yb20%, Tm 0.5%	I: BODIPY-FL II: Cy3.5 III: IR806	488, 517, 800, and 980	Between 50 and 100-fold (340–360 nm)	90
$NaYbF_4$/$NaYF_4$:Nd^{3+}	Cy7	808	15-fold (980 nm)	91
$NaYF_4$:Yb^{3+},Nd^{3+},Er^{3+}/$NaYF_4$:Nd^{3+}	Sulfonic-functionalized Cy7	808	17-fold (520 to 680 nm; Er^{3+} VIS emission)	92

triplets. This was accomplished by promoting the ISC in the dye *via* the adjustment of the UCNP composition. It was demonstrated that the triplet states in the dye antennas critically affect the brightness and stability of the dye–UCNP systems, thus providing relevant insight to overcome limitations found in previously reported materials. The IR-806-sensitized $NaYF_4$:Yb^{3+},Er^{3+} UCNPs underwent an adjustment of the Gd^{3+} content, from 0 to 30%, substituting the Y^{3+} ions. In particular, ISC within the dye was found to be enhanced by the larger spin–orbit coupling to Ln^{3+} ions near the surface of the UCNPs achieved by increasing the Gd^{3+} content (Fig. 4C). Furthermore, this enriched triplet population was responsible for a significant amount of energy transfer into the UCNPs. The overall result was a 30-fold enhancement in the UC emission. The main conclusion of this work is the possibility to concurrently optimize the LNP composition and the dye sensitization pathway to achieve maximum optical performance.

3.2.1. Rise of the concept from metal–organic complexes. The basic concept of organic molecules transferring absorbed optical energy to Ln^{3+}—no nanoparticle involved—can be tracked to the middle of the last century. A seminal study by S. I. Weissman in 1942[87] proved the efficient transfer of energy from organic ligands to Eu^{3+} ions in metal complexes. To this end, the early 2000s witnessed a blooming of the field of lanthanide complexes under the general idea of chromophores sensitizing Ln^{3+} emission (a concept also applied to supramolecular architectures and self-assembled compounds).[88]

By 2007, the first report was published by J. Zhang *et al.* for testing the concept of an organic dye acting as the antenna for lanthanide-doped (inorganic) nanoparticles.[93] This seminary paper portrayed the combination of the antenna effect provided by organic chromophores with the protection of Ln^{3+} given by an inorganic matrix. At the dawn of using antenna dyes for LNPs, the work from L. J. Charbonnière *et al.* must be highlighted.[94] The authors reported an increase in the emission of Eu^{3+} under 305 nm excitation of up to two orders of magnitude, as compared to the same Eu^{3+}-doped nanoparticles with no dye attached. A thorough photo-physical study demonstrated that such a large increase in the brightness of the LNP's luminescence, with a corresponding long-lived excited-state lifetime, was caused by a broad absorption in the near-UV and subsequent energy transfer to Eu^{3+} from $bipyCOO^-$ ligands tethered to the surface.

3.2.2. Organic antennas for UCNPs. History says that back in mid- and late-2000s, the genesis of the research interest around LNPs started with UCNPs based on the most classic Yb^{3+} (sensitizer)–Er^{3+} (activator) ion pair. The UC process is a low-output one; on top of the already described low absorption coefficient of Ln^{3+}-doped materials, the intrinsically poor efficiency of UC emission is to be added. This unfortunate synergy of brightness-limiting constraints makes UC a very attractive research area to test the potential of the organic antenna approach. Obviously, the application of organic (dye) antennas in the field of UC makes it necessary to find NIR-absorbing dyes that are able to properly funnel the NIR excitation energy to the Ln^{3+} sensitizers inside the UCNP matrix.

A remarkable milestone of this bubbling trend was published in 2012, when W. Zou *et al.* reported an enhancement by a factor of ~3300 of the overall sensitized UC emission of $NaYF_4$:Yb^{3+},Er^{3+} UCNPs by using the NIR-absorbing IR-806 organic dye as the antenna.[95] This dye was a carboxylic acid-functionalized derivative created by the nucleophilic substitution of the central chlorine atom in IR-780, which is a commercially available cyanine dye. The use of such a novel dye resulted in a blue-shift (806 nm) in the absorption maximum of the structure (LNP + dye) from 975 nm (*i.e.*, direct Yb^{3+} absorption) that is otherwise used for the optical excitation of the very same LNPs with no dye attached. The extinction coefficient of IR-806 at 806 nm was measured to be $\sim 5 \times 10^6$ times higher than that of $NaYF_4$:Yb^{3+},Er^{3+} nanoparticles at 975 nm. Interestingly, a set of photophysical control experiments demonstrated that ~50% of the photon energy initially absorbed by IR-806 is transferred to the Yb^{3+} and Er^{3+} energy-

accepting ions in the $NaYF_4$:Yb^{3+},Er^{3+} core. The glaring shortcoming of the proposed system was the remarkably large energy gap between the energy levels of the dye molecule and the Yb^{3+} ion. This fact limited the ET efficiency to support the UC process *via* the usual ET pathway (dye to Yb^{3+} and then to the Er^{3+} emitter). Moreover, the energy mismatch between the dye–Yb^{3+} energy levels may cause the ET performance to be undesirably temperature-dependent. Years later, G. Chen *et al.* introduced the concept of cascade energy UC to mitigate such a drawback. Using $NaYbF_4$:Tm^{3+}0.5%/$NaYF_4$:Nd^{3+} core/(active) shell UCNPs sensitized by different NIR-absorbing dyes as a model, they achieved a large enhancement in visible UC emission, efficacious ET, and surprisingly high (~19%) PLQY.[96]

As outstanding example from the materials viewpoint, in 2018, the work by C. Hazra *et al.* pushed the limits on the spectral range of excitation wavelength for dye-sensitized UCNPs.[97] In that work, the use of a water-dispersible dye absorbing above 1000 nm (IR-1061) to sensitize $NaYF_4$:Yb^{3+}30%/Tm^{3+}0.5%/$NaYF_4$:Yb^{3+}10% core/active shell UCNPs was proposed for the first time. Having the goal of proofing biomedical potential, the authors managed to encapsulate the as-synthesized NIR-absorbing dye in the polyoxomer Pluronic F68 (PF-68), thus rendering the dye water dispersible owing to the presence of hydroxyl groups. From a quantitative standpoint, a relatively modest ~3-fold enhancement in the 800 nm emission of the Tm^{3+} ion was reported from such IR-1061-sensitized UCNPs *via* the doping of Yb^{3+} ions (10% optimal) in the UCNP shell (*i.e.*, core/active shell architecture). Critically speaking, the performed excitation at 980 nm did not allow to fully profit from the IR-1061 absorption, which peaks at longer wavelengths within NIR-II. Moreover, the experiments also carried the drawbacks of a relatively strong water absorption at the chosen excitation wavelength.

3.2.3. Recent representative developments on organic antennas' sensitization of LNPs. There are diverse fields of application of the organic antenna approach for LNPs' absorption enhancement. In photovoltaics, UCNPs have been much sought after to expand the spectral working range of solar cells towards NIR, the spectral range to which almost half of the photons reaching Earth from the Sun belong. This active research line is very well exemplified by the work of S. Hao *et al.*[98] The authors built a core/shell nanoparticle, $NaYF_4$/Yb^{3+}10%,Er^{3+}2%/$NaYF_4$/Nd^{3+}30%, sensitized with the NIR-absorbing dye IR-783, and implemented it into a dye-sensitized solar cell (DSSC), achieving a 13.1% performance enhancement compared to the control cell in the absence of the UCNP-converting layer. Furthermore, efficiency improvement following NIR harvesting was quantified to be >3-fold higher than the one obtained with the core/shell UCNPs with no IR-783 dye attached. With a keen eye on the applications in real life, on checking the photostability of the system, the IR-783 dye was demonstrated to be photostable under AM1.5G simulated sunlight irradiation (100 min).

In the ever-growing field of integrated photo-electronics, systems based on dye-sensitized LNPs have also been actively developed. The work by J. Lee *et al.* is remarkable for several reasons,[90] starting from the use of a multi-dye organic antenna to sensitize the β-NaYF4 : 20%Yb^{3+},0.5%Tm^{3+} UCNPs. The three dyes were, namely, BODIPY-FL, Cy3.5, and IR-806, having in common their composition, comprising an energy harvesting aromatic fluorophore and a carboxylic acid for linkage to the UCNP. This game-changer approach widens the photon absorption window of such nanoparticles, from solely the NIR range (975 nm, when relying on just Yb^{3+} as the sensitizer) to the entire visible and NIR-I range (450–975 nm) (Fig. 4D). Such an expansion of the excitation range, encompassing photons that cannot be used in conventional UCNPs, maximized the utility of such Yb^{3+},Tm^{3+}-doped UCNPs. This is because a large photoabsorption bandwidth with high absorption coefficients increases the upconverted output emission intensity in the UV range. Moreover, the authors walked the extra mile in terms of material engineering, optimizing the sensitizer-ligand distance and the ratio between the different organic dyes, thus further increasing the efficiency of the sequential ET and UC processes (Fig. 4E). Finally, the third exciting aspect of the work lies in the application of such a fine-tuned nanosystem, in collaboration with ultraviolet (UV)-responsive photo-acid-generators (PAGs), as a new information security module in data storage devices with the function of unrecoverable data erasure. Because of the ultrathin nature of the so-built electronics, the entire system is deformable and can be integrated on various curvilinear surfaces including the human skin (Fig. 4F).

Not all the outstanding examples of organic antennas that improve absorption for LNPs have been developed for UC systems (Table 2). The current growing trend of developing NIR emitters for biomedical imaging owing to the deeper penetration, better optical contrast, and low tissue autofluorescence characterizing such spectral ''transparency window'' finds a fertile ground in LNPs. $NaYbF_4$/$NaYF_4$:Nd^{3+}60% nanoparticles were coupled with high-PLQY Cy7 dye in the work by Q. Liu *et al.* in 2018.[91] Starting from a pure $NaYbF_4$ emitter core, the authors augmented the Nd^{3+} doping concentration up to 60% in the outer shell, which is appreciably higher than in the case of most reported dye-sensitized systems. The architecture favoured the optically-absorbed energy that is transferred from the sensitizer (Cy7) to the emitters (Yb^{3+}) *via* intermediate ions (Nd^{3+}), the overall benefit being offered by a significant increase in the absorbance of the LNPs. Therefore, the brightness was increased, yielding a deeper imaging penetration (Fig. 4G). The relevance of this report lies also in how the water-solubility and biocompatibility of the nanosystem were addressed by wrapping the Cy7 dye–core/shell composite in phosphatidylcholine. This way, two of the key points of concern for biomedically-oriented LNPs were taken care of. This NIR-emitting (centred at 980 nm) material was applied *in vivo*, proving itself to be a promising imaging agent for fluorescence-guided surgery by way of its application in assisting in the procedure of peritumoral lymph node dissection. Notwithstanding the achievements of this paper, in line with the critical approach of this review, it is also worth noting that the characterization performed by the authors showed that coating with an inert shell would make energy transfer efficiency from Cy7 to Nd^{3+} relatively weak. This happens because the undoped outer shell

increases the physical distance between the (donor) organic molecules and the (acceptor) Ln^{3+} ions, thus hindering ET between the two species. Such incompatibility of the approaches severely limits the possibility to simultaneously implement organic antennas (for absorption betterment) together with the growth of an undoped outer protective shell (nowadays, a widely used method to improve the LNPs' quantum yield). This constitutes a limiting issue within the framework of LNPs' achievable brightness by the use of organic antennas, a matter discussed further in this review (*vide infra*).

Highlighting the most promising NIR-absorbing organic dyes, the above mentioned Cy7 has indeed made possible *in vivo* imaging even for UCNPs acting as imaging probes by emitting in the visible range. This result is remarkable, considering the sizeably lower tissue penetration depth in that wavelength range. Indeed, Nd^{3+}-based UCNPs sensitized with Cy7 demonstrated, as shown in the report by X. Zou *et al.*, *in vivo* lymphatic imaging at 540 nm under excitation at 808 nm (Fig. 4H).[92]

Finally, the report from W. Shao *et al.* in 2016 should also be analyzed within the current research trend to develop down-shifting LNPs for *in vivo* imaging, which emit at longer wavelengths (NIR-II and NIR-III spectral ranges, meaning 1000–1700 nm).[99] Therein, upon achieving NIR-II, III emission, the authors aimed at profiting from the assets already described above that arise from shifting the signal collection towards longer wavelengths (*i.e.*, deeper sub-skin penetration, better optical contrast, and higher signal-to-noise ratio). Thus, the $NaYF_4$:Yb^{3+}/X^{3+}/$NaYbF_4$/$NaYF_4$:Nd^{3+}, (X = null, Er, Ho, Tm, or Pr) core/shell/shell system, with indocyanine green (ICG) attached to the LNP surface, was designed to create a cascade ET pathway upon 700–860 nm optical excitation: ICG → Nd^{3+} (outer shell) → Yb^{3+} (inner shell) → Yb^{3+}/X^{3+} (core). The ICG antenna not only enhanced the overall brightness of the multiple-line emission of the LNPs by ~4 times but also provided the much broader excitation band than the LNPs had just by themselves. The proof-of-concept of NIR-II, III bioimaging was extended *in vivo* by means of subcutaneous injection of an aqueous suspension of phospholipid-encapsulated ICG-sensitized core/shell/shell LNPs, which allowed imaging in a mouse.

3.3. Semiconductors as light harvesters

The use of SCNs for the sensitization of Ln^{3+} emission follows the same principle of organic antennas: the semiconductor moiety should be able to absorb the optical energy and transfer it to the Ln^{3+} ions. The pivotal difference from the case of organic antennas is that the role of the dye's singlet/triplet states is herein played by the semiconductor's excited states. These can be localized excitonic levels, inter-bandgap levels, and charge trap states (Fig. 5A). SNCs have a molar absorption coefficient that is generally slightly larger than that of the dyes (up to 10^6 *vs.* up to 10^5 M^{-1} cm^{-1}).[100] However, the smaller size of dye molecules could mitigate this partial shortcoming since it is plausible to think that more dye molecules than SNCs could be accommodated on the surface of the LNPs (if the decoration LNPs with SNCs is the pursued approach). On the other hand, in the case of using SNCs, the final material is fully inorganic and hence, it is less prone to photobleaching and degradation in harsher environments.

Aside from the points above, a fair comparison should also include the efficiency of transfer between the light harvesting moiety (dye or SNC) and the lanthanide ion. Unfortunately, the very limited availability of these numbers makes it difficult to fairly compare the performance of the two approaches from this point of view.

The sensitization of Ln^{3+} through SNCs was accomplished *via* different approaches, such as the coupling of SNCs and LNPs, doping of Ln^{3+} in a SNC, and the synthesis of core/shell SNC/LNP structures (Table 3). Albeit these methods rely on a similar operation principle (Fig. 5A), they require attention to different variables.

3.3.1. Coupling of LNPs and SNCs. The main advantage of this method, compared to the doping of Ln^{3+} in SNCs, is the possibility to separately control the properties of the two nanoparticles. Moreover, the surface chemistry of the two species can be tuned independently, depending on the coupling strategy one wants to pursue. Two particularly relevant examples are represented by the amalgamation of NIR-absorbing SNCs of Ag_2S[101] or Ag_2Se[102] with LNPs to achieve brighter NIR or visible UC emission, respectively. Zhang *et al.* synthesized a hybrid Ag_2S–$NaYF_4$:Yb^{3+},Er^{3+} nanostructure, leveraging the electrostatic interaction between the positively charged surface of ligand-free LNPs and the carboxylic group of mercaptopropionic acid (MPA) on the surface of the Ag_2S SNCs. The resulting LNPs decorated with SNCs displayed a 17-fold increase in the Er^{3+} emission intensity (at 1550 nm) under 808 nm irradiation compared to direct 980 nm excitation of Yb^{3+} in the LNP (Fig. 5B). The authors also achieved *in vivo* tumour imaging in NIR-III under 808 nm excitation. They modified the surface of the LNPs with a glutathione-cleavable peptide; after cleavage took place in the tumour microenvironment, maleimide-modified Ag_2S SNCs injected in the mouse could bind to the LNPs *via* a "click" reaction, thus enabling the semiconductor mediated-sensitization of Er^{3+} emission. The result is an elegant demonstration of *in vivo* tumour imaging using a two-stage injection strategy, which allows increasing the emission intensity of the LNPs on demand. While developing this composite imaging probe, the authors also explored the effect of growing a protective shell on the LNPs. The observed trend echoes the results observed with dye sensitization, with luminescence enhancement through SNC decreasing almost linearly with the thickness of the shell. This is the result of the increased distance between the doped Yb^{3+} ions in the core (acceptors) and the Ag_2S SNCs tethered to the outer surface (donors). This assumption was confirmed by the regain in the luminescence enhancement upon doping Yb^{3+} ions also in the overgrown outer shell, thus again enabling efficient SNC-to-Yb^{3+} ET. It is interesting to note that the overall PLQY of the best performing sample only amounted to 0.16%. On the bright side, the composite retained up to 70% of the emission intensity upon continuous 808 nm irradiation for 60 min, which is in stark contrast to the 98% drop experienced by the analogue system featuring IR-806 dye molecules in place of Ag_2S SNCs. In a similar fashion, Song *et al.* prepared hydrophilic

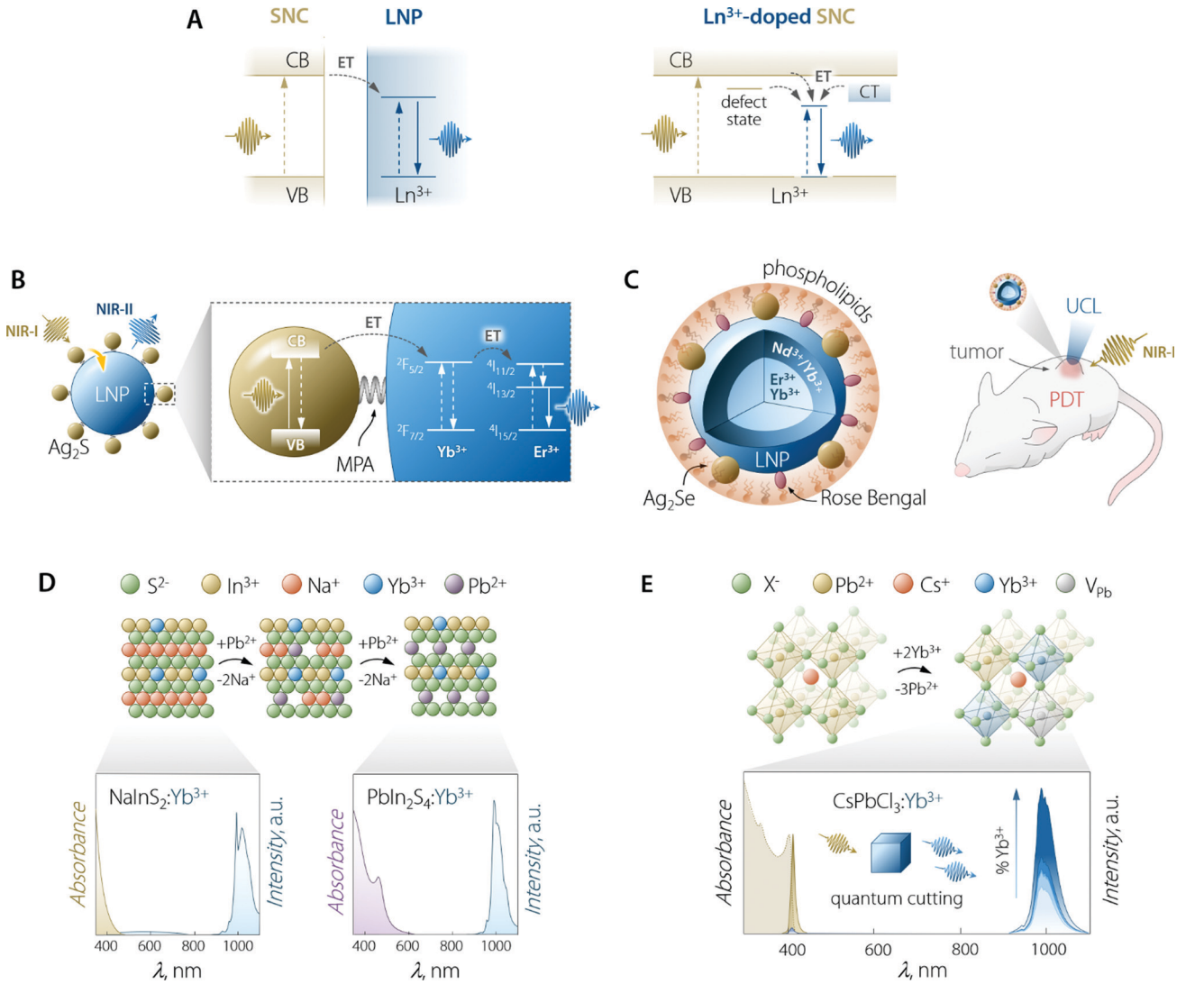

Fig. 5 Use of SNCs to increase the brightness of lanthanide emission. (A) Partial energy level diagrams to illustrate the sensitization mechanism between conjugated SNC and LNP moieties (left) and in the case of Ln^{3+}-doped SNC (right). In the latter case, CT means charge transfer state; dark yellow arrows indicate the ET processes and vertical lines are the electronic transitions. (B) Scheme of Ag_2S SNC-decorated Yb^{3+},Er^{3+}-doped LNPs along with the proposed energy transfer mechanism responsible for the sensitization of lanthanide NIR emission. MPA = 3-mercaptopropionic acid. Adapted with permission from ref. 101. Copyright 2020 American Chemical Society. (C) Scheme and means of operation as an optical probe and PDT agent of the Ag_2Se–LNP–Rose Bengal composite encapsulated in phospholipids. Adapted with permission from ref. 102. Copyright 2019 American Chemical Society. (D) Preparation of Yb^{3+}-doped $PbIn_2S_4$ SNCs and their optical properties. The cation exchange process to transform $NaInS_2$ into $PbIn_2S_4$ entails the substitution of two Pb^{2+} ions for each Na^+. Both $NaInS_2$:Yb^{3+} and $PbIn_2S_4$:Yb^{3+} feature host-sensitized Yb^{3+} emission around 1000 nm; however, upon passing from $NaInS_2$ to $PbIn_2S_4$, the absorption extends to longer wavelength, covering a good part of the visible spectrum. Adapted with permission from ref. 103. Copyright 2017 American Chemical Society. (E) Lanthanide doping scheme in Pb^{2+}-based halide perovskite SNCs along with the absorption and emission spectra of CsPbCl3:Yb^{3+} SNCs doped with increasing amounts of lanthanide ion (from 0 to 7.4%). Adapted with permission from ref. 104. Copyright 2018 American Chemical Society.

$NaYF_4$:Yb^{3+},Gd^{3+},Er^{3+}/$NaYF_4$:Yb^{3+},Nd^{3+} core/shell LNPs and co-encapsulated them with hydrophilic Ag_2Se SNCs in the micelles of phosphatidylcholine (Fig. 5C). On optimizing the SNC content in the micelles, the authors observed an 18-fold increase in the UC emission. Aside from using the system for imaging purposes, the authors displayed its suitability as a photodynamic therapy (PDT) agent when Rose Bengal (RB) was co-encapsulated in the micelles. In fact, the construct showed reactive oxygen species generation upon 808 nm irradiation thanks to the UC-mediated excitation of RB. It is also likely that the system displays NIR-III emission due to the presence of Er^{3+}, which could be harnessed for imaging purposes, as in the case of previously-discussed Ag_2S–$NaYF_4$:Yb^{3+},Er^{3+}. However, the authors did not explore this possibility. It is important to point out that the authors also investigated the photostability of the Ag_2Se SNCs *versus* a solution of IR-806 under 808 nm excitation. They observed a 10% emission intensity decrease in the case of SNCs, while the dye was almost completely photobleached. This evidence further corroborates the higher robustness of the LNP–SNCs systems compared with those based on organic antennas for Ln^{3+} sensitization.

Table 3 Summary of the main parameters describing the properties of the most relevant LNPs featuring SNC-enhanced emission described in Section 3.3

Coupling of SNCs and LNPs

LNP	SNC	Excitation wavelength (nm)	Enhancement (emission range)	Ref.
$NaYF_4$:Yb^{3+},Er^{3+}	Ag_2S	808	17 (NIR@1550 nm) [0.16% PLQY]	101
$NaYF_4$:Yb^{3+},Gd^{3+},Er^{3+}/$NaYF_4$:Yb^{3+},Nd^{3+}	Ag_2Se	808	18 (green)	102

Ln^{3+}-Doped SNCs

Ln^{3+}	Semiconductor	Excitation range (nm)	PLQY	Ref.
Eu^{3+}	CdS	<400	—	113
Tb^{3+}	CdSe	<500	0.03%	114
Yb^{3+}	CdSe	<600	—	115
Tb^{3+}, Eu^{3+}	ZnS, ZnSe, CdSe	ZnS: <410	ZnS:Tb^{3+}: 12% (overall), 5% (Tb^{3+}) ZnS:Eu^{3+}: 27% (overall), 0.01% (Eu^{3+})	116
Tb^{3+}	ZnO	<420	—	143
Eu^{3+}, Er^{3+}, Sm^{3+}	TiO_2	488	—	144
Eu^{3+}	In_2O_3	<400	—	120
Eu^{3+}, Tb^{3+}	Ga_2O_3	<250	Eu^{3+}: 0.1%	121
Yb^{3+}	$NaInS_2$, $PbIn_2S_4$ ($CdIn_2S_4$, $AgInS_2$)	<600	5% (λ_{ex} = 405 nm)	103
(Er^{3+}–Ce^{3+}, Nd^{3+}–Ce^{3+})	CaS	<300 (host), 400–500 (Ce^{3+})	Er^{3+}: 9.3%. Nd^{3+}: 7.7% [excited through Ce^{3+}]	122
Yb^{3+}	$CsPbCl_3$	<410	Up to 170% (λ_{ex} = 380 nm)	104
Ce^{3+}, Sm^{3+}, Eu^{3+}, Tb^{3+}, Dy^{3+}, Dy^{3+}, Er^{3+}, Yb^{3+}	$CsPbCl_3$	<410	Yb^{3+}: 142.7% Eu^{3+}: 27.2%	128
Yb^{3+}–Pr^{3+}–Ce^{3+}	$CsPbClBr_2$	<480	173% (overall)	129
Yb^{3+}, Er^{3+}	$Cs_2AgInCl_6$	<300	Yb^{3+}: 3.6% Er^{3+}: 0.05%	134
Yb^{3+}	$Cs_2AgBiCl_6$ $Cs_2AgBiBr_6$	<420 <520	<1%	135
Eu^{3+}	$Cs_3Bi_2Br_3$	<425	42.4% (overall), approx. 28% (Eu^{3+})	136

Other structures

Ln^{3+}-Doped material	Semiconductor	Excitation wavelength (nm)	PLQY	Ref.
YF_3:Yb^{3+}/LuF_3 (shell material)	InP (core material)	440 (and 760)	0.1–0.5%	142

Nonetheless, as mentioned above, one of the main disadvantages of this approach lies in the necessity of the SNCs to be in close proximity to the sensitizer ions for the ET to effectively take place. This means that only superficial ions in the LNP can accept energy from the SNCs. This reduces the possibility of growing a passivating shell on the LNPs, as also underscored earlier in this minireview in the case of dye-sensitization of LNP emission (see Section 3.2.3). All these considerations have also been demonstrated in the reverse case of LNP-to-SNC ET[105,106] and they pose limitations in the design of the final nanostructure.

3.3.2. Doping of Ln^{3+} in SNCs. This approach yields a single entity rather than a composite nanostructure where two or more particles are bound together. However, this compactness comes at the cost of more stringent requirements to meet in the material design and from a synthetic standpoint. Recently, we have discussed in detail this specific approach in a dedicated review;[107] therefore, here, we will only outline the main aspects to be considered. Notably, the following considerations are valid generally when attempting the doping of any nanoparticle with Ln^{3+} ions. First, a host material apt for substitutional Ln^{3+} doping should feature cationic sites with high coordination number (CN),[108] such as those with octahedral or cubic geometries. In addition, similar ionic radius and oxidation state favor the substitution of the native cation in the SNC with Ln^{3+}. Once a suitable host material has been chosen, the preparation of Ln^{3+}-doped SNCs could proceed through several synthetic methods, such as growth doping,[109] nucleation doping,[110] cation exchange,[111] and diffusion doping.[112] All these methods have in common the need to control the reactivity of different ions in the reaction environment so as to promote the incorporation of Ln^{3+} in the lattice. This is no easy task and often a combination of coordinating molecules should be employed to ensure that Ln^{3+} ions successfully enter and reside in the SNC lattice. Clearly, all these considerations should be complemented by attention to the relative energetic position of the semiconductor excited states and the Ln^{3+} emitting state, as previously mentioned. This set of requirements makes the preparation of Ln^{3+}-doped SNCs challenging. Moreover, there is an element of serendipity that is constituted by the defects possibly introduced by the doping of Ln^{3+} in the lattice. These defects can generate localized interbandgap trap states for charge carriers, which either contribute to non-radiative recombination or act as effective bridge between the host and doped Ln^{3+}.

Early attempts to prepare Ln^{3+}-doped SNCs focused on the use of binary semiconductors, such as CdS,[113] CdSe,[114,115] and ZnS.[116] However, these lattices are far from ideal in this context

since therein Cd^{2+} and Zn^{2+} occupy low-CN sites (tetrahedral). Moreover, these ions feature different size and oxidation state compared to Ln^{3+}. In fact, most of the works attempting Ln^{3+} incorporation in the SNC lattice mainly report the evidence of surface absorption of the dopant ions.[117] Some success was obtained by the group of Meijerink, who managed to immobilize Yb^{3+} ions on the surface of the CdSe SNCs *via* ion adsorption, followed by the overgrowth of a thin Se layer.[115] Numerous studies have been reported on the incorporation of Ln^{3+} in oxide-based semiconductor nanoparticles, such as ZnO,[118] TiO_2,[119] In_2O_3,[120] and Ga_2O_3.[121] Although host sensitization is achieved in these materials, the efficiency is generally poor and the absorption of the semiconductor moiety lies in the UV-vis part of the spectrum. Interestingly, Gamelin and co-workers reported the incorporation of Ln^{3+} in the lattice of colloidal ternary SNCs (Fig. 5D).[103] Their approach involved the use of $NaInS_2$ as the host material—a ternary semiconductor where In^{3+} resides in an octahedral environment. The similar ionic radius of this cation compared to Ln^{3+}, along with same oxidation state (3+), allowed for the effective incorporation of Yb^{3+} in the lattice. The advantage of using a ternary system where cations with different properties (*i.e.*, Na^+ and In^{3+}) granted the possibility to perform selective cation exchange to fine-tune the optical properties of the Ln^{3+}-doped SNCs. The authors showed that Na^+ can be substituted by Cd^{2+}, Ag^+, and Pb^{2+}. Exchange with the latter cation afforded partially-exchanged $PbIn_2S_4$:Yb^{3+} SNCs, which exhibited extended visible absorption and a maximum PLQY of 5%.

Other host materials that grant effective Ln^{3+} doping are alkaline-earth semiconductors (AESs) such as CaS and SrS.[109,122–124] The large cationic radius of the alkaline earths, along with their high CN, allows for their substitution by lanthanides. Often, Ce^{3+} is doped in these hosts, while europium takes its divalent state. Hence, albeit host sensitization is observed, efficient direct excitation of doped lanthanide ions is generally realized. For instance, Zhang *et al.* recently prepared CaS:Ce^{3+},Er^{3+} and CaS:Ce^{3+},Nd^{3+} featuring NIR emission under UV-blue excitation. Energy transfer from Ce^{3+} to the second Ln^{3+} enabled bright emission (PLQY of 9.3 and 7.7%, respectively, for Er^{3+} and Nd^{3+}). After transferring these LNPs to water with the aid of phospholipids, the authors managed to sense H_2O_2 and H_2O_2-producing disease marker xanthine in water. The detection of these species was afforded by the quenching of Ln^{3+} emission in the presence of hydrogen peroxide.

This section would not be complete without mentioning halide perovskites. In the past few years, semiconductors of the family $CsPbX_3$ (where X = Cl, Br, I) have become the staple for Ln^{3+} doping in SNCs, with unmatched results in terms of host-sensitized photoluminescence efficiency.[108] Halide perovskites, in general, feature octahedral sites, which offer an ideal coordination environment for Ln^{3+}. In lead-based systems, doping with Ln^{3+} proceeds through the substitution of three Pb^{2+} for every two incorporated lanthanides.[104,125] To maintain the charge balance, a Pb^{2+} vacancy (V_{Pb}) is also introduced. The most energetically-favourable configuration of the resulting defect complex (Ln^{3+}–V_{Pb}–Ln^{3+}) is shown in Fig. 5E. Hence, Ln^{3+} doping of halide perovskites proceeds through the creation of defects and the possibility to successfully dope this material hinges on the tolerance that it possesses towards defects, both structure- and emission-wise.[126,127] Several Ln^{3+} (Ce^{3+}, Sm^{3+}, Eu^{3+}, Tb^{3+}, Dy^{3+}, Dy^{3+}, Er^{3+}, Yb^{3+}) were doped in $CsPbCl_3$ SNCs by Pan *et al.*,[128] observing increased overall PLQY (exciton + Ln^{3+} emission) compared to the undoped system. Stunningly, the PLQY in the case of Yb^{3+} doping overcame 100%. Because of their high conversion efficiency and the ideal overlap of Yb^{3+} emission with silicon absorption, Yb^{3+}-doped halide perovskites are thus envisioned as ideal conversion materials in photovoltaic devices. Indeed, conversion layers for silicon and $Cu(In,Ga)(S,Se)_2$ cells[129,130] and quantum cutting luminescent solar concentrators (QC-LSC) have been prepared using Ln^{3+}-doped lead halide perovskite SNCs. This quantum cutting phenomenon was further investigated by Milstein *et al.*, who described it with the help of low-temperature photoluminescence study on La^{3+}-doped SNCs.[104] The authors explained quantum cutting as assisted by shallow defect states below the conduction band, thus effectively bridging the electronic states of the SNC and the Ln^{3+}. In a following study, Li *et al.* modelled this quantum cutting phenomenon and explained it in light of the higher density of states (DOS) at the CB edge featured by Pb^{2+} located close to the Yb^{3+} ions. This increased DOS favours strong localized absorption in correspondence of the transition metal ion, followed by energy transfer to the two nearby Yb^{3+}.[125] Ln^{3+}-doped lead-based perovskite SNCs were also used for preparing with-light emitting diodes, wherein blue-emitting GaN chips were coated with polymeric dispersions of, for *e.g.*, $CsPbCl_3$:Ce^{3+},Eu^{3+} (ref. 128) or $CsPbCl_{1.8}Br_{1.2}$:Ce^{3+},Mn^{2+}.[131] Despite Pb^{2+}-based halide perovskites' showcasing excellent luminescent performance, the presence of lead in their composition, in hand with the poor chemical resistance towards moisture, poses major concerns in terms of the toxicity and environmental impact.[132] Ln^{3+}-doping has been shown to improve the stability of $CsPbX_3$[133] but their foreseeable applicability remains limited mainly to water-free environments. In search for more sustainable alternatives, the incorporation of Ln^{3+} in other lead-free mixed perovskites has been performed too, using hosts such as halide double perovskites (*e.g.*, $Cs_2AgInCl_6$[134] and $Cs_2AgBiCl_6$[135]) and $Cs_3Bi_2Br_3$.[136,137] To this end, Eu^{3+}-doped SNCs of the latter material have been prepared by Ding *et al.*, who employed them in aqueous media for Cu^{2+} detection, a rare instance of the use of perovskites in water.[136] However, the emission efficiency of Pb^{2+}-free systems is often lower compared to the one featured by lead-containing ones. Lastly, the absorption of halide perovskites generally cannot be effectively tuned towards the red-NIR part of the spectrum, thus further limiting the versatility in terms of the working wavelength range, particularly foreseeing applications in the biomedical field where NIR working capabilities (both absorption and emission) are key.

Despite the challenges of doping Ln^{3+} in SNCs, an additional advantage of this avenue is the possibility of exploiting the host-to-metal charge transfer (CT) phenomena to sensitize the activator luminescence.[138,139] According to the model proposed by Dorenbos[140] (and validated several times experimentally), Ln^{3+} ions that are more likely to give rise to CT are Eu^{3+} and Yb^{3+},

followed by Sm^{3+} and Tm^{3+}. This is because of the lower-lying ground state of their divalent form (Ln^{2+}) compared to other lanthanides. This subject is rather complex and its thorough explanation lies beyond the scope of the present review. The interested reader is redirected to the body of work from Dorenbos (see, for example, ref. 141). The important aspect to consider is that when Ln^{3+} ions are doped in hosts composed of relatively polarizable anions (such as S^{2-} and Se^{2-} as opposed to O^{2-} and F^{-}), absorption corresponding to the CT band occurs at lower energies. This observation opens the door to the possibility of tuning the position of CT-related light absorption by controlling the host composition.

Lastly, this approach for combining Ln^{3+} and SNCs allows for core/shell architectures to be prepared. The passivation of the surface therefore becomes possible, aiming for higher PLQY. We foresee exciting scenarios ahead in this avenue.

3.3.3. Core/shell architectures. A unique case is represented by the work of Swabeck *et al.*, where a YF_3:Yb^{3+} shell was grown over an InP SNC core.[142] Passivation of the system with a further shell of LuF_3 alleviated solvent molecule-induced quenching. This approach allowed achieving Yb^{3+} emission under 440 nm excitation thanks to ET from the SNC core to the Yb^{3+} ions in the YF_3 shell with PLQY in the range of 0.1–0.5%. The sensitization appears to proceed *via* the involvement of an intermediate trap state (likely an Yb^{3+}-induced surface state), which acts as a bridge between the InP excited states and the lanthanide ion. This claim was supported by the observation of Yb^{3+} emission, also under excitation with 760 nm light, a wavelength corresponding to the energy of the trap-related emission recorded upon 440 nm excitation. We foresee that structures with reverse architecture could be prepared in the future, where LNP represents the core and a shell of semiconductor material is overgrown. The shell would act not only as a sensitizer moiety but simultaneously as a protective barrier for the emitted Ln^{3+} ions against the quenchers (*i.e.*, molecules with high-energy vibrations). Further shelling performed on the first semiconductor shell could further reduce non-radiative losses.

4. Conclusion and perspective

In this minireview, we have assessed the state-of-the-art of three families of approaches to improve the brightness (mainly by increasing the absorption capability) of lanthanide-doped nanoparticles. These strategies entail the use of (i) plasmonic species, (ii) organic antennas, and (iii) semiconductor nanocrystals. From our critical literature survey, we can draw several general conclusions:

– The interest around the production of brightly-emitting nanoparticles based on lanthanide ions is vivid. Efforts towards this direction are driven by the possibility of broadening the applicability of these unique luminescent species in fields such as lighting, photovoltaics, and bioimaging.

– Enhancement of the light absorption properties of lanthanide ions appears to be the decisive step in undertaking the pursuit of increased emission brightness of these species. Strategies to achieve this goal are constantly being honed both from a physical and chemical standpoint. A better understanding of the mechanisms involved in brightness enhancement by way of absorption enhancement allows for a more rational and effective design of the material. On the other hand, new materials and synthetic strategies are being proposed, thus opening a host of new opportunities.

– Despite the advancements witnessed in the preparation of more intensely-emitting lanthanide-based nanoparticles, we are far from the performance and reliability of other luminescent species, such as fluorescent small molecules, quantum dots, or even lanthanide complexes. Yet, it is encouraging to observe that dye-sensitized lanthanide-based nanoparticles have been applied with unrivalled results in cellular imaging thanks to improved brightness and sensitivity compared to other fluorophores.[145,146] However, in general, there is plenty of room for improvement in terms of brightness enhancement as well as chemical and photostability.

Regarding the specific strategies discussed in this review, the following conclusions have been reached.

– Coupling with plasmonic materials is one of the most exploited approaches to enhance the emission intensity of lanthanide-based nanoparticles. Yet, in colloidal systems, the degree of control that can be exerted over the reciprocal position of the two moieties is limited. The combination of wet-chemistry methods and metal deposition has already proven to be a useful hybrid approach for the preparation of unique architectures. In these nanosystems, the electromagnetic field is concentrated within the lanthanide-doped nanoparticle, thus allowing for maximum luminescence enhancement. It is expected that similar results can be achieved harnessing methods to decorate selectively different sites of plasmonic nanostructures.[147] Lanthanide-doped materials can be deposited, for instance, at the tip of the gold nanorods, where the longitudinal plasmonic mode results in maximal localized enhancement of the electromagnetic field. On top of that, the use of plasmonic materials other than noble metals should be further investigated. For example, materials with plasmonic resonance located deeper in the NIR (*e.g.*, >1400 nm) could be used to enhance the absorption and/or emission of lanthanide ions at these wavelengths, which are relatively unexplored. Copper chalcogenides, indium tin oxide, and LaB_6 nanoparticles could serve that purpose. We also observed a lack of studies where the lanthanide-doped moiety is optimized in terms of the dopant type, concentration, and relative positioning. The mastery achieved in preparing complex structures with multiple shells, wherein different dopants are spatially segregated for maximum optical performance, has grown in the past few years.[148,149] Therefore, it should be employed also in the design of nanomaterials with even brighter plasmon-enhanced luminescence. We also note that the body of literature dealing with brightness enhancement of LNPs by betterment of the absorption capabilities of Ln^{3+} is limited. This is unfortunate since this approach is the one anticipated to yield higher enhancements and thus, more efforts should be put in this direction. One of the possible battlefields

where nanostructures based on LNPs and PNPs could be deployed is biomedicine for theranostic (therapeutic + diagnostic) purposes. Enhanced upconversion luminescence and downshifting emission can be harnessed to photoinitiate chemical reactions *in situ* and imaging, respectively. However, the presence of the plasmonic part could be a double-edged sword owing to its light-to-heat conversion capability; if, on the one hand, this effect can be harnessed for photothermal therapy, on the other hand, unwanted and uncontrolled heating can be generated upon irradiation.

– The most pressing shortcomings toward the consolidation of the use of organic antennas for addressing the low absorption of LNPs are basically three. Firstly, opting for this approach (absorption enhancement) limits the possibility to prepare nanoparticle architectures with an undoped outer shell, which is known to lead to an improvement of the quantum yield through quenching suppression. The undoped shell both alleviates the quenching phenomena, arising from surface defects as well as from the interaction between Ln^{3+} and solvent molecules with vibrational modes resonant with Ln^{3+} transitions. However, the distance imposed by the shell between the Ln^{3+} and the surface, where organic molecules anchor makes the antenna approach poorly effective, as successful energy transfer requires the involved species to be at close range. A possible solution to this conundrum could surge from the use of an optically-active organic polymer able to act as the antenna for Ln^{3+}, simultaneously providing strong isolation to the very same Ln^{3+} from the vibrational modes of solvent (water) molecules.

The second limitation is directly related to the structural stability and long-term robustness of the whole antenna-nanoparticle construct. In a majority of the published reports, the binding stability of the dye onto the nanoparticle surface remains largely a matter pending further study, along with the unknown photostability of the dye-sensitized LNP. To that end, no comparative studies have been systematically performed for the most functional "anchoring" methods, *i.e.*, covalent bonding, electrostatic attraction, and physical absorption. In particular, the unknown stability of the bond between the dye and the nanoparticle curbs the application of these nanocomposites in the *in vivo* biomedical arena. Indeed, upon injection in the specimen, these LNPs would find themselves in a potentially aggressive environment that could possibly induce detachment of the dye molecules.

Lastly, the third relevant factor imposing constraints is the number of dyes per nanoparticle. In the published works, this number has often been reported to be less than 1000 : 1, thus posing a threshold to the light-harvesting ability of dye-sensitized LNPs. In other words, there seems to exist an upper limit of dye molecules per nanoparticle, above which the molecules are more likely to transfer energy between them than to the Ln^{3+} inside the LNP matrix.

As a general comment, there is still a sort of "thematic-scope gulf", keeping disciplines away between researchers working on the physical properties of lanthanide ions (particularly, the luminescence side of LNPS) and organic chemists, in particular, those interested in the soft-chemistry facet of colloidal dispersions. However, it is reasonable to think that this gap will continue to be gradually bridged, especially when considering previous relevant cases such as the very travelled research road of dye-sensitized semiconductor solar cells.

– The research line dealing with the use of semiconductor materials to sensitize the emission of lanthanide ions is by far the one that is gaining greater momentum thanks to the advent on the scene of halide perovskites. The optical and structural properties of these materials make them utterly suitable for the preparation of Ln^{3+}-doped nanoparticles with bright emission. Provided that lead-based species are the ones performing the best, future effort should be put in the development of LNPs based on heavy metal-free materials that are also resistant to moisture (hence more broadly applicable in aqueous environments). Bismuth-based and halide double perovskites are amongst the most promising materials in these regards. Following this path, on the one hand, concerns about the toxicity of the material would be mitigated. On the other, more stable and water-resistant species will ensure their broader applicability in field such as light-emitting diodes, photovoltaics, and biomedicine. Aside from perovskites, it is foreseeable that novel, efficient lanthanide-doped semiconductor nanocrystals could be produced, leveraging the strategy of ion exchange, following the example set by the group of Gamelin.[103] Ternary semiconductors represent the ideal canvas for this approach as they allow orthogonal manipulation of their composition (*i.e.*, selective exchange of one or the other metal ion). Once these strategies will be mastered, taking one page from the book of quantum dots, the preparation of core/shell architectures is the natural successive step. The minimization of surface quenching phenomena that will result is envisaged to increase the emission brightness of doped lanthanides to an even higher degree. Core/shell structures, where the core is an LNP and the shell is constituted of semiconductor materials, are also expected to be designed (although lattice mismatch between the materials involved might pose serious limitations to the realizability of these structures). Regarding other strategies, the coupling of pre-synthesized semiconductor nanocrystals and lanthanide-doped nanoparticles could provide a means to more finely tune the optical properties of the two moieties in a separate way. On the negative side, the nature of the interparticle energy transfer mechanisms involved in the sensitization process poses limits in terms of the maximum distance between the energy donor (semiconductor nanocrystal) and the acceptors (lanthanide ions doped in the nanoparticle). Notwithstanding this, it is often easier to prepare such composite structures rather than pursuing lanthanide doping in semiconductors, given the knowledge gained over the recent years of nanoparticle surface functionalization. This knowledge also allows to agilely tune the affinity (*i.e.*, dispersibility) of the composite towards different environments depending on the application sought after, a task more challenging in the case of using organic dyes, most of which are not hydrophilic. Consequently, we propose that the coupling of semiconductor nanocrystals and lanthanide-doped nanoparticles could bring exciting results in the next few years, particularly in the biomedical context.

All in all, the journey in the chase of brighter lanthanide-doped nanoparticles presents several opportunities and it is far from being at its end. While the avenues described above have

been walked so far independently, it is also possible that they will intersect, joining forces quite literally for a brighter tomorrow. Case in point, the coupling of plasmonic nanoparticles and lanthanide-doped nanocrystals can be performed with the goal of simultaneously profiting from host sensitization and Purcell effect. The decoration of lanthanide-doped nanoparticles with both plasmonic species and organic dyes could be performed too. These are just some examples but the list of combined methods is expected to quickly become longer.

Like we have mentioned throughout Section 3, the application fields that would mainly benefit from the availability of lanthanide-doped inorganic nanoparticles are photovoltaics, lighting, sensing, and biomedicine. Of course, each area necessitates specific requirements to be met in terms of optical and physicochemical features, as well as the toxicity profile of the nanosystem. For this reason, it is plausible to think that different strategies will provide species suitable for different applications. What we are convinced of is that lanthanide-doped nanoparticles made brighter *via* the methods reviewed herein will play a pivotal role in several fields.

Conflicts of interest

There are no conflicts to declare.

Acknowledgements

The authors thank Prof. A. Fernández-Domínguez (UAM) for helpful discussion about plasmonic concepts. R. M. is grateful to the European Commission for the financial support through the Marie Skłodowska-Curie Grant agreement no. 797945 "LANTERNS". A. B. acknowledges funding from Comunidad Autónoma de Madrid through TALENTO grant ref. 2019-T1/IND-14014. This work was partially supported by the Ministerio de Economía y Competitividad de España (MAT2016-75362-C3-1-R), by the Ministerio de Ciencia e Innovación (PID2019-106211RB-I00), by the Instituto de Salud Carlos III (PI16/00812), and by the Comunidad Autónoma de Madrid (B2017/BMD-3867RENIMCM). Additional funding was provided by the European Union's Horizon 2020 FET Open programme under grant agreement no. 801305 (NanoTBTech).

References

1 M. Poliakoff, A. D. J. Makin, S. L. Y. Tang and E. Poliakoff, *Nat. Chem.*, 2019, **11**, 391–393.
2 R. Marin, G. Brunet and M. Murugesu, *Angew. Chem., Int. Ed.*, 2019, DOI: 10.1002/anie.201910299.
3 D. N. Woodruff, R. E. Winpenny and R. A. Layfield, *Chem. Rev.*, 2013, **113**, 5110–5148.
4 S. F. Himmelstoss and T. Hirsch, *Methods Appl. Fluoresc.*, 2019, **7**, 022002.
5 C. D. S. Brites, S. Balabhadra and L. D. Carlos, *Adv. Opt. Mater.*, 2018, **7**, 1801239.
6 B. del Rosal, E. Ximendes, U. Rocha and D. Jaque, *Adv. Opt. Mater.*, 2017, **5**, 1600508.
7 A. Skripka, V. Karabanovas, G. Jarockyte, R. Marin, V. Tam, M. Cerruti, R. Rotomskis and F. Vetrone, *Adv. Funct. Mater.*, 2019, **29**, 1807105.
8 Z. Chen, X. Wang, S. Li, S. Liu, H. Miao and S. Wu, *ChemPhotoChem*, 2019, **3**, 1077–1083.
9 F. Vetrone, R. Naccache, A. Zamarron, A. Juarranz de la Fuente, F. Sanz-Rodriguez, L. Martinez Maestro, E. Martin Rodriguez, D. Jaque, J. Garcia Sole and J. A. Capobianco, *ACS Nano*, 2010, **4**, 3254–3258.
10 C. D. S. Brites, B. Zhuang, M. L. Debasu, D. Ding, X. Qin, F. E. Maturi, W. W. Y. Lim, W. Soh, J. Rocha, Z. Yi, X. Liu and L. D. Carlos, *J. Phys. Chem. Lett.*, 2020, **11**, 6704–6711.
11 A. Lay, C. Siefe, S. Fischer, R. D. Mehlenbacher, F. Ke, W. L. Mao, A. P. Alivisatos, M. B. Goodman and J. A. Dionne, *Nano Lett.*, 2018, **18**, 4454–4459.
12 M. He, X. Pang, X. Liu, B. Jiang, Y. He, H. Snaith and Z. Lin, *Angew. Chem., Int. Ed.*, 2016, **128**, 4352–4356.
13 J. Day, S. Senthilarasu and T. K. Mallick, *Renewable Energy*, 2019, **132**, 186–205.
14 J.-C. G. Bünzli, *Coord. Chem. Rev.*, 2015, **293–294**, 19–47.
15 S. V. Eliseeva and J. C. Bunzli, *Chem. Soc. Rev.*, 2010, **39**, 189–227.
16 O. Laporte and W. F. Meggers, *J. Opt. Soc. Am.*, 1925, **11**, 464–564.
17 F. Auzel, *Chem. Rev.*, 2004, **104**, 139–173.
18 X. Qin, X. Liu, W. Huang, M. Bettinelli and X. Liu, *Chem. Rev.*, 2017, **117**, 4488–4527.
19 F. Wang, X. Xue and X. Liu, *Angew. Chem., Int. Ed.*, 2008, **47**, 906–909.
20 Q. Dou and Y. Zhang, *Langmuir*, 2011, **27**, 13236–13241.
21 J. Huang, J. Li, X. Zhang, W. Zhang, Z. Yu, B. Ling, X. Yang and Y. Zhang, *Nano Lett.*, 2020, **20**, 5236–5242.
22 L. Lei, D. Chen, J. Xu, R. Zhang and Y. Wang, *Chem. – Asian J.*, 2014, **9**, 728–733.
23 T. Cheng, R. Marin, A. Skripka and F. Vetrone, *J. Am. Chem. Soc.*, 2018, **140**, 12890–12899.
24 X. Chen, D. Peng, Q. Ju and F. Wang, *Chem. Soc. Rev.*, 2015, **44**, 1318–1330.
25 D. Hudry, I. A. Howard, R. Popescu, D. Gerthsen and B. S. Richards, *Adv. Mater.*, 2019, **31**, e1900623.
26 Y. Fan, P. Wang, Y. Lu, R. Wang, L. Zhou, X. Zheng, X. Li, J. A. Piper and F. Zhang, *Nat. Nanotechnol.*, 2018, **13**, 941–946.
27 M. Zhao, B. Li, Y. Wu, H. He, X. Zhu, H. Zhang, C. Dou, L. Feng, Y. Fan and F. Zhang, *Adv. Mater.*, 2020, **32**, e2001172.
28 X. Li, Z. Guo, T. Zhao, Y. Lu, L. Zhou, D. Zhao and F. Zhang, *Angew. Chem., Int. Ed.*, 2016, **55**, 2464–2469.
29 D. Peng, Q. Ju, X. Chen, R. Ma, B. Chen, G. Bai, J. Hao, X. Qiao, X. Fan and F. Wang, *Chem. Mater.*, 2015, **27**, 3115–3120.
30 R. Marin, G. Sponchia, P. Riello, R. Sulcis and F. Enrichi, *J. Nanopart. Res.*, 2012, **14**, 886.
31 M. Back, E. Trave, R. Marin, N. Mazzucco, D. Cristofori and P. Riello, *J. Phys. Chem. C*, 2014, **118**, 30071–30078.
32 K. Trejgis and L. Marciniak, *Phys. Chem. Chem. Phys.*, 2018, **20**, 9574–9581.

33 M. Saboktakin, X. Ye, U. K. Chettiar, N. Engheta, C. B. Murray and C. R. Kagan, *ACS Nano*, 2013, **7**, 7186–7192.
34 K. T. Lee, J. H. Park, S. J. Kwon, H. K. Kwon, J. Kyhm, K. W. Kwak, H. S. Jang, S. Y. Kim, J. S. Han, S. H. Lee, D. H. Shin, H. Ko, I. K. Han, B. K. Ju, S. H. Kwon and D. H. Ko, *Nano Lett.*, 2015, **15**, 2491–2497.
35 W. Park, D. Lu and S. Ahn, *Chem. Soc. Rev.*, 2015, **44**, 2940–2962.
36 A. Skripka, T. Cheng, C. M. S. Jones, J. Marques-Hueso, R. Marin and F. Vetrone, *Nanoscale*, 2020, **12**, 17545–17554.
37 D. Lu, S. K. Cho, S. Ahn, L. Brun, C. J. Summers and W. Park, *ACS Nano*, 2014, **8**, 7780–7792.
38 S. Rohani, M. Quintanilla, S. Tuccio, F. De Angelis, E. Cantelar, A. O. Govorov, L. Razzari and F. Vetrone, *Adv. Opt. Mater.*, 2015, **3**, 1606–1613.
39 J. He, W. Zheng, F. Ligmajer, C. F. Chan, Z. Bao, K. L. Wong, X. Chen, J. Hao, J. Dai, S. F. Yu and D. Y. Lei, *Light: Sci. Appl.*, 2017, **6**, e16217.
40 H. Li, Q. Deng, B. Liu, J. Yang and B. Wu, *RSC Adv.*, 2016, **6**, 13343–13348.
41 Z. Li, L. Wang, Z. Wang, X. Liu and Y. Xiong, *J. Phys. Chem. C*, 2011, **115**, 3291–3296.
42 P. Yuan, Y. H. Lee, M. K. Gnanasammandhan, Z. Guan, Y. Zhang and Q. H. Xu, *Nanoscale*, 2012, **4**, 5132–5137.
43 P. Kannan, F. Abdul Rahim, R. Chen, X. Teng, L. Huang, H. Sun and D. H. Kim, *ACS Appl. Mater. Interfaces*, 2013, **5**, 3508–3513.
44 P. Kannan, F. A. Rahim, X. Teng, R. Chen, H. Sun, L. Huang and D.-H. Kim, *RSC Adv.*, 2013, **3**, 7718–7721.
45 S. Fischer, D. Kumar, F. Hallermann, G. von Plessen and J. C. Goldschmidt, *Opt. Express*, 2016, **24**, A460–A475.
46 Y. Xue, C. Ding, Y. Rong, Q. Ma, C. Pan, E. Wu, B. Wu and H. Zeng, *Small*, 2017, **13**, 1701155.
47 D. Mendez-Gonzalez, S. Melle, O. G. Calderon, M. Laurenti, E. Cabrera-Granado, A. Egatz-Gomez, E. Lopez-Cabarcos, J. Rubio-Retama and E. Diaz, *Nanoscale*, 2019, **11**, 13832–13844.
48 Q. Zhan, X. Zhang, Y. Zhao, J. Liu and S. He, *Laser Photonics Rev.*, 2015, **9**, 479–487.
49 F. Kang, J. He, T. Sun, Z. Y. Bao, F. Wang and D. Y. Lei, *Adv. Funct. Mater.*, 2017, **27**, 1701842.
50 Y. Chen, K. Munechika and D. S. Ginger, *Nano Lett.*, 2007, **7**, 690–696.
51 D. M. Wu, A. Garcia-Etxarri, A. Salleo and J. A. Dionne, *J. Phys. Chem. Lett.*, 2014, **5**, 4020–4031.
52 A. Das, C. Mao, S. Cho, K. Kim and W. Park, *Nat. Commun.*, 2018, **9**, 4828.
53 H. Zhang, Y. Li, I. A. Ivanov, Y. Qu, Y. Huang and X. Duan, *Angew. Chem., Int. Ed.*, 2010, **49**, 2865–2868.
54 M. Kanehara, H. Koike, T. Yoshinaga and T. Teranishi, *J. Am. Chem. Soc.*, 2009, **131**, 17736–17737.
55 J. Li, W. Zhang, C. Lu, Z. Lou and B. Li, *Nanoscale Horiz.*, 2019, **4**, 999–1005.
56 D. Zhou, D. Liu, W. Xu, Z. Yin, X. Chen, P. Zhou, S. Cui, Z. Chen and H. Song, *ACS Nano*, 2016, **10**, 5169–5179.
57 T. M. Mattox, A. Agrawal and D. J. Milliron, *Chem. Mater.*, 2015, **27**, 6620–6624.
58 Y. Ma, L. Zhang, L. Wang, L. Wang and H. Chen, *Anal. Methods*, 2017, **9**, 2977–2982.
59 Y. Qin, Z. Dong, D. Zhou, Y. Yang, X. Xu and J. Qiu, *Opt. Mater. Express*, 2016, **6**, 1942–1955.
60 H. Xing, W. Bu, S. Zhang, X. Zheng, M. Li, F. Chen, Q. He, L. Zhou, W. Peng, Y. Hua and J. Shi, *Biomaterials*, 2012, **33**, 1079–1089.
61 T. Jiang, J. Li, W. Qin and J. Zhou, *J. Lumin.*, 2014, **156**, 164–169.
62 M. Rai, S. K. Singh, A. K. Singh, R. Prasad, B. Koch, K. Mishra and S. B. Rai, *ACS Appl. Mater. Interfaces*, 2015, **7**, 15339–15350.
63 S. Liu, G. Chen, T. Y. Ohulchanskyy, M. T. Swihart and P. N. Prasad, *Theranostics*, 2013, **3**, 275–281.
64 S. Wu, N. Duan, Z. Shi, C. Fang and Z. Wang, *Talanta*, 2014, **128**, 327–336.
65 M. Runowski, *J. Lumin.*, 2017, **186**, 199–204.
66 M. Sun, L. Xu, W. Ma, X. Wu, H. Kuang, L. Wang and C. Xu, *Adv. Mater.*, 2016, **28**, 898–904.
67 C. Zhang and J. Y. Lee, *J. Phys. Chem. C*, 2013, **117**, 15253–15259.
68 L. Sudheendra, V. Ortalan, S. Dey, N. D. Browning and I. M. Kennedy, *Chem. Mater.*, 2011, **23**, 2987–2993.
69 A. Priyam, N. M. Idris and Y. Zhang, *J. Mater. Chem.*, 2012, **22**, 960–965.
70 Y. Song, G. Liu, J. Wang, X. Dong and W. Yu, *Phys. Chem. Chem. Phys.*, 2014, **16**, 15139–15145.
71 D. Yin, C. Wang, J. Ouyang, X. Zhang, Z. Jiao, Y. Feng, K. Song, B. Liu, X. Cao, L. Zhang, Y. Han and M. Wu, *ACS Appl. Mater. Interfaces*, 2014, **6**, 18480–18488.
72 F. Zhang, G. B. Braun, Y. Shi, Y. Zhang, X. Sun, N. O. Reich, D. Zhao and G. Stucky, *J. Am. Chem. Soc.*, 2010, **132**, 2850–2851.
73 W. Ge, X. R. Zhang, M. Liu, Z. W. Lei, R. J. Knize and Y. Lu, *Theranostics*, 2013, **3**, 282–288.
74 Y. Zhang, J. Wang, F. Nan and Q.-Q. Wang, *RSC Adv.*, 2018, **8**, 20056–20060.
75 B. A. R. Aiken, W. P. Hsu and E. Matijevic, *J. Am. Ceram. Soc.*, 1988, **71**, 845–853.
76 Y. Huang, F. Rosei and F. Vetrone, *Nanoscale*, 2015, **7**, 5178–5185.
77 C. Wang, C. Xu, L. Xu, C. Sun, D. Yang, J. Xu, F. He, S. Gai and P. Yang, *J. Mater. Chem. B*, 2018, **6**, 2597–2607.
78 C. Wang, L. Xu, J. Xu, D. Yang, B. Liu, S. Gai, F. He and P. Yang, *Dalton Trans.*, 2017, **46**, 12147–12157.
79 F. Xu, H. Gao, J. Liang, S. Jin, J. Zhao, Y. Liu, H. Zhang, Z. Zhang and Y. Mao, *Ceram. Int.*, 2019, **45**, 21557–21563.
80 T. Hinamoto, H. Takashina, H. Sugimoto and M. Fujii, *J. Phys. Chem. C*, 2017, **121**, 8077–8083.
81 T. Hinamoto, T. Higashiura, H. Sugimoto and M. Fujii, *J. Phys. Chem. C*, 2019, **123**, 25809–25815.
82 N. J. Greybush, M. Saboktakin, X. Ye, C. Della Giovampaola, S. J. Oh, N. E. Berry, N. Engheta, C. B. Murray and C. R. Kagan, *ACS Nano*, 2014, **8**, 9482–9491.

83 G. Bao, S. Wen, G. Lin, J. Yuan, J. Lin, K.-L. Wong, J.-C. G. Bünzli and D. Jin, *Coord. Chem. Rev.*, 2021, **429**, 213642.
84 D. L. Dexter, *J. Chem. Phys.*, 1953, **21**, 836–850.
85 Z. Q. You, C. P. Hsu and G. R. Fleming, *J. Chem. Phys.*, 2006, **124**, 044506.
86 D. J. Garfield, N. J. Borys, S. M. Hamed, N. A. Torquato, C. A. Tajon, B. Tian, B. Shevitski, E. S. Barnard, Y. D. Suh, S. Aloni, J. B. Neaton, E. M. Chan, B. E. Cohen and P. J. Schuck, *Nat. Photonics*, 2018, **12**, 402–407.
87 S. I. Weissman, *J. Chem. Phys.*, 1942, **10**, 214–217.
88 J. P. Leonard, C. B. Nolan, F. Stomeo and T. Gunnlaugsson, *Photochemistry and Photophysics of Coordination Compounds II*, Springer-Verlag Berlin Heidelberg, 2007, ch. 142, pp. 1–43.
89 X. Wang, R. R. Valiev, T. Y. Ohulchanskyy, H. Agren, C. Yang and G. Chen, *Chem. Soc. Rev.*, 2017, **46**, 4150–4167.
90 J. Lee, B. Yoo, H. Lee, G. D. Cha, H. S. Lee, Y. Cho, S. Y. Kim, H. Seo, W. Lee, D. Son, M. Kang, H. M. Kim, Y. I. Park, T. Hyeon and D. H. Kim, *Adv. Mater.*, 2017, **29**, 1603169.
91 Q. Liu, X. Zou, Y. Shi, B. Shen, C. Cao, S. Cheng, W. Feng and F. Li, *Nanoscale*, 2018, **10**, 12573–12581.
92 X. Zou, M. Xu, W. Yuan, Q. Wang, Y. Shi, W. Feng and F. Li, *Chem. Commun.*, 2016, **52**, 13389–13392.
93 J. Zhang, C. M. Shade, D. A. Chengelis and S. Petoud, *J. Am. Chem. Soc.*, 2007, **129**, 14834–14835.
94 L. J. Charbonnière, J.-L. Rehspringer, R. Ziessel and Y. Zimmermann, *New J. Chem.*, 2008, **32**, 1055–1059.
95 W. Zou, C. Visser, J. A. Maduro, M. S. Pshenichnikov and J. C. Hummelen, *Nat. Photonics*, 2012, **6**, 560–564.
96 G. Chen, J. Damasco, H. Qiu, W. Shao, T. Y. Ohulchanskyy, R. R. Valiev, X. Wu, G. Han, Y. Wang, C. Yang, H. Agren and P. N. Prasad, *Nano Lett.*, 2015, **15**, 7400–7407.
97 C. Hazra, S. Ullah, Y. E. Serge Correales, L. G. Caetano and S. J. L. Ribeiro, *J. Mater. Chem. C*, 2018, **6**, 4777–4785.
98 S. Hao, Y. Shang, D. Li, H. Agren, C. Yang and G. Chen, *Nanoscale*, 2017, **9**, 6711–6715.
99 W. Shao, G. Chen, A. Kuzmin, H. L. Kutscher, A. Pliss, T. Y. Ohulchanskyy and P. N. Prasad, *J. Am. Chem. Soc.*, 2016, **138**, 16192–16195.
100 U. Resch-Genger, M. Grabolle, S. Cavaliere-Jaricot, R. Nitschke and T. Nann, *Nat. Methods*, 2008, **5**, 763–775.
101 W. Zhang, T. Chen, L. Su, X. Ge, X. Chen, J. Song and H. Yang, *Anal. Chem.*, 2020, **92**, 6094–6102.
102 D. Song, S. Chi, X. Li, C. Wang, Z. Li and Z. Liu, *ACS Appl. Mater. Interfaces*, 2019, **11**, 41100–41108.
103 S. E. Creutz, R. Fainblat, Y. Kim, M. C. De Siena and D. R. Gamelin, *J. Am. Chem. Soc.*, 2017, **139**, 11814–11824.
104 T. J. Milstein, D. M. Kroupa and D. R. Gamelin, *Nano Lett.*, 2018, **18**, 3792–3799.
105 R. Marin, L. Labrador-Paéz, A. Skripka, P. Haro-González, A. Benayas, P. Canton, D. Jaque and F. Vetrone, *ACS Photonics*, 2018, **5**, 2261–2270.
106 S. Bhuckory, E. Hemmer, Y.-T. Wu, A. Yahia-Ammar, F. Vetrone and N. Hildebrandt, *Eur. J. Inorg. Chem.*, 2017, 5186–5195.
107 R. Marin and D. Jaque, *Chem. Rev.*, 2020, DOI: 10.1021/acs.chemrev.0c00692, accepted.
108 W. J. Mir, T. Sheikh, H. Arfin, Z. Xia and A. Nag, *NPG Asia Mater.*, 2020, **12**, 9.
109 Y. Zhao, F. T. Rabouw, T. van Puffelen, C. A. van Walree, D. R. Gamelin, C. de Mello Donega and A. Meijerink, *J. Am. Chem. Soc.*, 2014, **136**, 16533–16543.
110 M. Makkar, A. Saha, S. Khalid and R. Viswanatha, *J. Phys. Chem. Lett.*, 2019, **10**, 1992–1998.
111 L. De Trizio and L. Manna, *Chem. Rev.*, 2016, **116**, 10852–10887.
112 V. A. Vlaskin, C. J. Barrows, C. S. Erickson and D. R. Gamelin, *J. Am. Chem. Soc.*, 2013, **135**, 14380–14389.
113 J. Planelles-Aragó, E. Cordoncillo, R. A. S. Ferreira, L. D. Carlos and P. Escribano, *J. Mater. Chem.*, 2011, **21**, 1162–1170.
114 D. A. Chengelis, A. M. Yingling, P. D. Badger, C. M. Shade and S. Petoud, *J. Am. Chem. Soc.*, 2005, **127**, 16752–16753.
115 R. Martin-Rodriguez, R. Geitenbeek and A. Meijerink, *J. Am. Chem. Soc.*, 2013, **135**, 13668–13671.
116 P. Mukherjee, C. M. Shade, A. M. Yingling, D. N. Lamont, D. H. Waldeck and S. Petoud, *J. Phys. Chem. A*, 2011, **115**, 4031–4041.
117 A. A. Bol, R. van Beek and A. Meijerink, *Chem. Mater.*, 2002, **14**, 1121–1126.
118 V. Kumar, O. M. Ntwaeaborwa, T. Soga, V. Dutta and H. C. Swart, *ACS Photonics*, 2017, **4**, 2613–2637.
119 V. Štengl, S. Bakardjieva and N. Murafa, *Mater. Chem. Phys.*, 2009, **114**, 217–226.
120 Q. Xiao, Y. Liu, L. Liu, R. Li, W. Luo and X. Chen, *J. Phys. Chem. C*, 2010, **114**, 9314–9321.
121 T. Wang, A. Layek, I. D. Hosein, V. Chirmanov and P. V. Radovanovic, *J. Mater. Chem. C*, 2014, **2**, 3212–3222.
122 M. Zhang, W. Zheng, Y. Liu, P. Huang, Z. Gong, J. Wei, Y. Gao, S. Zhou, X. Li and X. Chen, *Angew. Chem., Int. Ed.*, 2019, **58**, 9556–9560.
123 D. C. Rodríguez Burbano, E. M. Rodríguez, P. Dorenbos, M. Bettinelli and J. A. Capobianco, *J. Mater. Chem. C*, 2014, **2**, 228–231.
124 J. Wang, Y. Zhu, C. A. Grimes and Q. Cai, *Nanoscale*, 2019, **11**, 12497–12501.
125 X. Li, S. Duan, H. Liu, G. Chen, Y. Luo and H. Ågren, *J. Phys. Chem. Lett.*, 2019, **10**, 487–492.
126 J. Kang and L. W. Wang, *J. Phys. Chem. Lett.*, 2017, **8**, 489–493.
127 J.-P. Ma, Y.-M. Chen, L.-M. Zhang, S.-Q. Guo, J.-D. Liu, H. Li, B.-J. Ye, Z.-Y. Li, Y. Zhou, B.-B. Zhang, O. M. Bakr, J.-Y. Zhang and H.-T. Sun, *J. Mater. Chem. C*, 2019, **7**, 3037–3048.
128 G. Pan, X. Bai, D. Yang, X. Chen, P. Jing, S. Qu, L. Zhang, D. Zhou, J. Zhu, W. Xu, B. Dong and H. Song, *Nano Lett.*, 2017, **17**, 8005–8011.
129 D. Zhou, R. Sun, W. Xu, N. Ding, D. Li, X. Chen, G. Pan, X. Bai and H. Song, *Nano Lett.*, 2019, **19**, 6904–6913.
130 D. Zhou, D. Liu, G. Pan, X. Chen, D. Li, W. Xu, X. Bai and H. Song, *Adv. Mater.*, 2017, **29**, 1704149.

131 G. Pan, X. Bai, W. Xu, X. Chen, D. Zhou, J. Zhu, H. Shao, Y. Zhai, B. Dong, L. Xu and H. Song, *ACS Appl. Mater. Interfaces*, 2018, **10**, 39040–39048.
132 Z. Wang, Z. Shi, T. Li, Y. Chen and W. Huang, *Angew. Chem., Int. Ed.*, 2017, **56**, 1190–1212.
133 L. Wang, H. Zhou, J. Hu, B. Huang, M. Sun, B. Dong, G. Zheng, Y. Huang, Y. Chen, L. Li, Z. Xu, N. Li, Z. Liu, Q. Chen, L. D. Sun and C. H. Yan, *Science*, 2019, **363**, 265–270.
134 W. Lee, S. Hong and S. Kim, *J. Phys. Chem. C*, 2019, **123**, 2665–2672.
135 N. Chen, T. Cai, W. Li, K. Hills-Kimball, H. Yang, M. Que, Y. Nagaoka, Z. Liu, D. Yang, A. Dong, C. Y. Xu, R. Zia and O. Chen, *ACS Appl. Mater. Interfaces*, 2019, **11**, 16855–16863.
136 N. Ding, D. Zhou, G. Pan, W. Xu, X. Chen, D. Li, X. Zhang, J. Zhu, Y. Ji and H. Song, *ACS Sustainable Chem. Eng.*, 2019, **7**, 8397–8404.
137 Y. Zhu, J. Zhu, H. Song, J. Huang, Z. Lu and G. Pan, *J. Rare Earths*, 2020, DOI: 10.1016/j.jre.2020.06.007.
138 O. M. ten Kate, H. T. Hintzen, P. Dorenbos and E. van der Kolk, *J. Mater. Chem.*, 2011, **21**, 18289–18294.
139 M. A. Klik, T. Gregorkiewicz, I. V. Bradley and J. P. Wells, *Phys. Rev. Lett.*, 2002, **89**, 227401.
140 P. Dorenbos, *J. Phys.: Condens. Matter*, 2003, **15**, 8417–8434.
141 P. Dorenbos, *Opt. Mater.*, 2017, **69**, 8–22.
142 J. K. Swabeck, S. Fischer, N. D. Bronstein and A. P. Alivisatos, *J. Am. Chem. Soc.*, 2018, **140**, 9120–9126.
143 G. L. Kabongo, G. H. Mhlongo, T. Malwela, B. M. Mothudi, K. T. Hillie and M. S. Dhlamini, *J. Alloys Compd.*, 2014, **591**, 156–163.
144 D. Falcomer, M. Daldosso, C. Cannas, A. Musinu, B. Lasio, S. Enzo, A. Speghini and M. Bettinelli, *J. Solid State Chem.*, 2006, **179**, 2452–2457.
145 M. Cardoso Dos Santos, J. Goetz, H. Bartenlian, K. L. Wong, L. J. Charbonnière and N. Hildebrandt, *Bioconjugate Chem.*, 2018, **29**, 1327–1334.
146 C. Charpentier, V. Cifliku, J. Goetz, A. Nonat, C. Cheignon, M. Cardoso Dos Santos, L. Frances-Soriano, K. L. Wong, L. J. Charbonniere and N. Hildebrandt, *Chem. – Eur. J.*, 2020, **26**, 14602–14611.
147 F. Wang, S. Cheng, Z. Bao and J. Wang, *Angew. Chem., Int. Ed.*, 2013, **52**, 10344–10348.
148 L. Labrador-Paez, E. C. Ximendes, P. Rodriguez-Sevilla, D. H. Ortgies, U. Rocha, C. Jacinto, E. Martin Rodriguez, P. Haro-Gonzalez and D. Jaque, *Nanoscale*, 2018, **10**, 12935–12956.
149 Y. Fan, L. Liu and F. Zhang, *Nano Today*, 2019, **25**, 68–84.

